A non-structural fuzzy decision method developed for organic Rankine cycles used in liquid-dominated geothermal fields of medium/high temperature

Na Zhang[1], Qinggang Wang[1], Zhibin Yu[2], Guopeng Yu[2,*]

1. School of Civil Engineering and Architecture, East China Jiaotong University, Nanchang, China

2. James Watt School of Engineering, University of Glasgow, United Kingdom, G12 8QQ

Corresponding author: Guopeng.Yu@glasgow.ac.uk

Abstract

A reliable decision-making method is of great importance for the designing of a practical and efficient organic Rankine cycle (ORC) system employed to exploit geothermal energy. This paper develops a three-level non-structural fuzzy decision algorithm for the comprehensive evaluation of a geo-fluid driven trans-critical ORC (TORC) system on the basis of a progressive system performance hierarchy, involving environmental characteristics, safety, thermodynamic and techno-economic performance. Two representative geothermal reservoirs with medium (GR-I) and high (GR-II) temperature are investigated to realize and validate the proposed method. Four mathematical models and six working fluids with thirteen indexes are developed to fulfill the performance evaluation and decision-making courses. Parametric analysis results of the decision criteria are conducted including specific net out power (AP_{net}), thermal efficiency (η_t), exergy efficiency (η_e), heat transfer area per net output power (APR) and electricity production cost (EPC), and the different performance of TORC for GR-I and GR-II are fully revealed. As for the GR-I, the result of the three-level fuzzy decision ranking order is R142b, R134a, R290, R1270, R227ea and R143a. In regard to the GR-II, it's R142b, R1270, R134a, R290, R227ea and R143a. Both show that R142b performs best. In the GR-I and GR-II, R142b obtains the maximal AP_{net} of 110.94kW/(kg·s^{-1}) and 198.14kW/(kg·s^{-1}), the maximal η_t of 14.05% and 14.43%, the maximal η_e of 51.42% and 42.90%, the minimal APR of 0.262(m^2/kW) and 0.185(m^2/kW), the minimal EPC of 0.030($/(kW·h)) and 0.022($/(kW·h)).

Summarily, this three-level fuzzy decision evaluation method can provide important guidance and decisive solution by concisely display the pros and cons for each ORC scheme of geothermal resource utilization.

Keywords: Geothermal energy; Trans-critical ORC; Three-level performance evaluation; non-structural fuzzy decision method

Introduction

Dramatic increase in energy consumption attributes to the fast population expansion and economic growth. A large proportion of energy supply for electricity is currently generated by the combustion of organic fuels, which leads to the growing greenhouse effect and air pollution concerns. For the purpose of human society sustainable progress, renewable resource like geothermal is capable of providing the majority of activities energy with power production, heating and cooling applications [1]. However, the cumulative installed geothermal power capacity in the globe is only increasing from 7.92GW at 2001 to 13.93GW at 2019, which is far away from the growth rate of solar and wind [2]. The conflict between the huge reserve and exploitation of geothermal resources lies in the expensive initial investments [3]. Besides that, the geothermal utilization also relies on the public awareness of environment protection as well as the efficiency enhancement of technologies [1].

The organic Rankine cycle (ORC) has been regarded as a preferred rational solution to harvesting energy from all kinds of heat sources such as waste heat and geothermal reservoirs [4]. Studies on ORC-based waste heat system are devoted to optimizing the engine performance. Liang et al. [5] proposed a small-scale waste heat driven cooling system which integrated supercritical CO_2 power cycle and trans-critical CO_2 refrigeration cycle to recover the waste heat from internal combustion engine and provide cooling energy for refrigerated truck. Li et al. [6] presented a novel framework for analyzing the off-design performance of CO_2 trans-critical power cycle and applied in the heavy-duty truck engine. Song et al. [7] conducted a one-dimensional off-design performance analysis of ORC system by optimizing the turbine aerodynamic model. Wang et al. [8] investigated the part-load performance of ORC system based on the engine waste heat recovery with varying evaporation pressure, condensing condition, working fluid and cycle structure, which revealed that the slower the output power decrease, the better the performance.

Normally, the geothermal heat is categorized as high, medium and low temperature with temperature ranges of >220℃, 220-100℃ and 100-70℃, respectively [9]. The thermodynamic as well as the techno-economic indicators are the major criteria for making investment decisions, which show direct relevance with the utilization benefit of geothermal energy. Summarizing from previous work about geothermal ORC system, researchers are committed to simulating the actual operating process for improving the system thermodynamic and economic performance. Astolfi et al. [10, 11] completed thermodynamic and techno-economic assessments of the ORCs (subcritical, trans-critical, saturated, superheated, regenerative and non-regenerative) for medium temperature geothermal brines. Regarding cycle efficiency and electricity cost as objective functions, the optimization results suggested deploying different cycle layouts that needed to consider the suitable working conditions and economic parameters simultaneously. Vetter et al. [12] analyzed the potential relevance between the maximal net output power and working fluid critical temperature with geothermal fluid temperature in the subcritical and trans-critical ORC system. It found out the highest net output power appeared when the ratio of working fluid critical temperature and geothermal fluid temperature was 0.8. Additionally, the geothermal ORC combined with different subsystem is a feasible way to make system thermo-economic performance better. Sun et al. [13] investigated the effect of pinch point temperature difference (PPTD) on the geothermal ORC thermo-economic performance. The optimization results showed that the optimal evaporation temperature and the heat transfer area

per unit power output decreased with increasing PPTD. The levelized cost of electricity and the dynamic payback period reached minimal when PPTD was 7℃. Meng et al. [14] further explored the interaction between the evaporation and flash temperature on recovering heat from medium temperature geothermal brine. Cakici et al. [15] performed the energy and exergy analysis of trans-critical regenerative ORC system combined with parabolic trough solar collectors. The integrated system net output power increased while the electricity and exergy efficiency decreased compared to single system, and R134a yielded outstanding thermodynamic performance with an increment of the geothermal water inlet temperature and collector areas.

Since the ORC system efficiency depends on the refrigerants properties, researchers also have paid much attention on optimal selection of working fluids with thermodynamic laws assessments. Moloney et al. [4] investigated thermodynamic performance of recuperative trans-critical ORC system for a range of medium to high temperature geothermal reservoirs, indicating that R1233zd(E), R600, R601a, R601, R601b performed the best among twenty working fluids when taken plant efficiency as optimization parameters. Wang et al. [16] developed a working fluid selection methodology mainly based on the thermodynamic performance for the subcritical, superheated, and trans-critical ORC system, utilizing supercritical CO_2 as heat extraction medium in the high temperature geothermal reservoir. The working fluid was recommended when the net output power, specific net output power, thermal efficiency and exergy efficiency were simultaneously equal or greater than their median value. Furthermore, some studies adopt evaluation tool which takes account of environmental properties of working fluids. Heberle et al. [17] qualified the potential of low GWP working fluids like R600, R601a, R290, R1233zd, R1234yf as alternatives for fluorinated fluids like R245fa during the life cycle assessment in the binary geothermal power plant. Judging by the exergy and environmental analysis results, the low GWP working fluids had less effect on environment and higher exergy efficiency in comparison to fluorinated fluids, and the two-stage subcritical ORC and trans-critical ORC manifested better than one-stage subcritical ORC system. For the purpose that avoids the occurrence of refrigerant leakage and guarantees the stable working

conditions of geothermal ORC system, it depends on selecting working fluids with environmental friendly, safety, low flammability and excellent thermodynamic and techno-economic characteristics.

Plenty of investigations are discretely concerned about environmental, thermodynamic and economic performance of geothermal ORC system. But they might neglect the internal relationship between the effective factors. Consequently, a few literatures started to search for multi-objective optimization techniques. Jankowski et al. [18] investigated the influence of geothermal brine salinity on the performance in the subcritical ORC power plant. Taking the minimal heat transfer area and maximal exergy efficiency as the multi-objective parameters under Genetic Algorithm, the Pareto point demonstrated that the heat transfer area increased 8% and exergy efficiency decreased 5% with an increment in salinity. Bina et al. [19] constructed multi-criteria fuzzy TOPSIS decision making method for selecting most favorable cycle configuration in geothermal power plant, covering exergy efficiency, thermal efficiency, net output power, production cost, total cost rate the five indicators. From the thermo-economic perspective and interval Shannon's entropy weighting calculation, the ORC system with internal heat exchanger ranked the first. Wang et al. [20] explored the relationship of pinch point temperature difference (PPTD) between evaporator and condenser in the thermo-economic optimization process of subcritical ORC system. Based on the Analytic Hierarchy Process (AHP) method which cared about the energy output, energy output efficiency and economic criteria, it determined the best working fluid for 150℃ hot water was R11 and the optimal ratio of PPTD was from 1.25 to 1.5.

Although numerous studies have discussed the optimization and evaluation process, the objective indicators just covered relatively limited side and couldn't give a thorough analysis of the overall ORC system performance. The non-structural fuzzy decision method is widely used as an efficient approach for comprehensive evaluation, which considers the indexes interrelation and provides intuitive comparison of the assessed schemes. Zhou et al. [21] adopted non-structural fuzzy decision method for pre-design process of compact heat exchangers which united the thermodynamic, economic and mechanical the three levels evaluation indexes. In the light of the third level evaluation result, the first alternative for sulfuric acid solution cooler was plate-fin heat exchanger fabricated by PTFE.

It can be found that most previous investigations about geothermal ORC system incline to take basis of first and second laws analysis with thermodynamics, focusing on these aspects of thermodynamic and techno-economic performance evaluation, system structure and layout, objective optimization and working fluid selection. Regarding the simulated results of highest net output power or lowest initial investment Cost as criterion to determine the best ORC system scheme. However, the assessment process tends to concentrate on one level decision criteria like thermodynamic indicators, which fails to integrate the comprehensive influence of techno-economic and social benefit indicators on the system whole performance. It may lead the pre-designed scheme to an unachievable goal and cause irretrievable loss to the investors.

Thus, this paper aims at developing an efficient and practical decision-making method, i.e. a three-level non-structural fuzzy decision method, based on comprehensive performance evaluation of the ORC employed for typical geothermal reservoirs. During the whole assessment procedures, six working fluids and three levels of performance are investigated, including the safety and environmental property as the first level, thermodynamic performance as the second level and the techno-economic performance as the third level. A non-structural fuzzy decision-making method is then developed based on the three-level assessment to eventually implement practical and reliable decision-making for the geothermally driven ORC systems.

1 System description

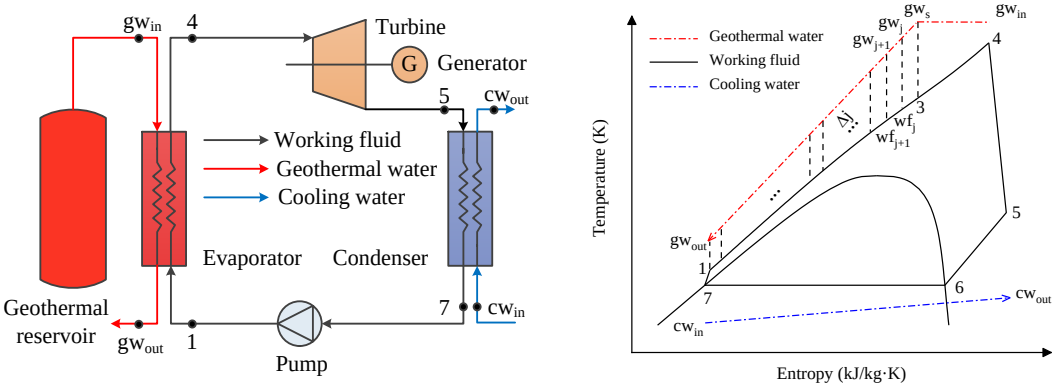

Fig. 1. Schematic and T-s diagram of TORC system

Table 1 Operating conditions of TORC system

Parameter	Value
GR-I wellhead temperature, T_{gwin-1} (℃)	182.23
GR-I wellhead pressure, P_{gw-1} (MPa)	1.06
GR-I wellhead mass flow rate, m_{gw-1} (kg/s)	13.64
GR-II wellhead temperature, T_{gwin-2} (℃)	224.37
GR-II wellhead pressure, P_{gw-2} (MPa)	2.52
GR-II wellhead mass flow rate, m_{gw-2} (kg/s)	11
Condensing temperature, T_{cond} (℃)	35
Cooling water inlet temperature, T_{cwin} (℃)	20
Evaporator pinch point temperature, $T_{pinch-e}$ (℃)	10
Condenser pinch point temperature, $T_{pinch-c}$ (℃)	5
Turbine isentropic efficiency, $\eta_{turbine}$	0.75
Pump isentropic efficiency, η_{pump}	0.7
Dead state temperature, T_{dead} (℃)	20
Dead state pressure, P_{dead} (MPa)	0.101

The geothermal reservoirs under investigation in this work are located in the Aluto Langano geothermal field of Ethiopia, which is recognized as a medium/high temperature liquid-dominated geothermal field in eastern Africa. Two typical and active geothermal reservoirs (i.e., Geothermal Reservoir I and Reservoir II) are chosen as heat source for the proposed system. They produced two-phase, fluid-dominated wellhead discharge, and the discharge data from wellhead tests are gathered and listed in Table 1. Wellhead pressure, temperature and mass flow rate are tested in situ. Instead of choosing the basic sub-critical ORC pattern, the trans-critical ORC (TORC) is determined for its higher energy efficiency, lower exergy loss and modest pressure requirement [22]. The primary TORC system working conditions constructed for working fluids in the GR-I (182.23℃) and GR-II (224.37℃) are nearly identical except the investigated evaporation pressure and turbine inlet temperature and flow channels in heat exchangers. Table 1 lists the detailed value of relevant parameters for TORC design and construction. As demonstrated in the semantic definition of TORC, the working fluid is compressed to exceed critical pressure via pump. And it absorbs heat from geothermal water to vaporize until it reaches the highest temperature during the courses of evaporation. Then, the supercritical working fluid discharges into the turbine to produce output shaft work which can be employed for power generation. After expansion, the subcritical overheated vapor is condensed into saturated liquid by cooling water before flowing into the pump to accomplish the next cycle. The schematic and T-s diagram is illustrated in Fig. 1. The T-s diagram also shows the segment-iterative

process of seeking pinch point temperature between the heat source and working fluids.

Table 2 Fluid characteristics [4, 16]

Working Fluid	Thermodynamic Property						Environmental Property			
	M /(kg·kmol^{-1})	T_b /℃	T_{de} /K	T_{cr} /K	P_{cr} /MPa	Behavior	Safety Level	ALT/Year	ODP	GWP/(100 years)
R227ea	170.0289	-16.341	475	374.9	2.925	dry	A1	38.9	0	3320
R134a	102.032	-26.0738	455	374.21	4.0593	wet	A1	13.4	0	1430
R143a	84.041	-47.2406	650	345.857	3.761	wet	A2L	47.1	0	4470
R290	44.0956	-42.1138	650	369.89	4.2512	wet	A3	0.034	0	5
R1270	42.0797	-47.6192	575	364.211	4.555	wet	A3	0.001	0	1.8
R142b	100.495	-9.1233	470	410.26	4.055	isentropic	A2	17.2	0.065	2310

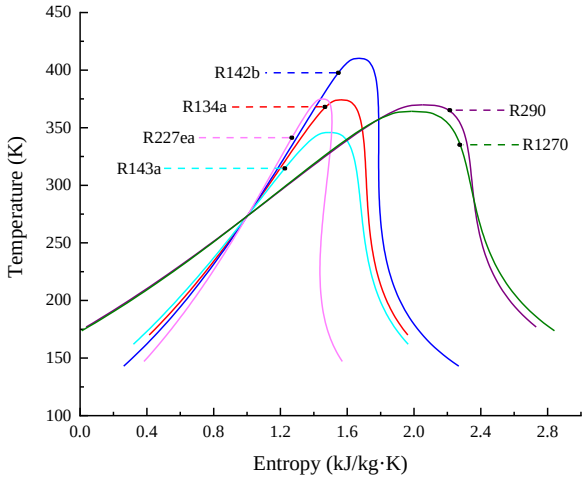

Fig. 2. T-s diagram of selected working fluids

The operating process of TORCs for two geothermal reservoirs are simulated in MATLAB with six picked working fluids, the environmental and thermodynamic characteristics of each working fluid are displayed in Table 2 and Fig. 2. The principals for selecting working fluids are subject to the safety level, atmospheric life time (ALT), ozone depletion potential (ODP) and global warming potential (GWP).

For the safety level, A and B imply the toxicity grades while B is higher than A. Number 1, 2, 2L and 3 indicate flammability level and increase progressively. ALT represents existing time at the atmosphere if leakage of refrigerant happens, ODP means the ozone consumption with refrigerant diffusing into ozone layer, and GWP indicates the potential of temperature increase in the global world caused by inappropriately release of refrigerant. With regard to the four environmental indicators, the smaller value the better performance. And the iteration ranges of turbine inlet temperature are higher than critical temperature but lower than working fluids decomposition temperature. Furthermore, the assumptions stated as below are taken into consideration:

- Each TORC system is operating steadily.
- No impurity like silica exists in the geothermal water, as result its outlet temperature is allowed for lower than 70℃.
- The pressure drop and heat losses are neglected during each part of performing process.
- The ambient temperature and pressure are 20℃ and 101kPa.
- The pinch point temperature in the evaporator and condenser are 10℃ and 5℃ respectively.

2 Mathematical modelling

2.1 Thermodynamic model

Based on the first and second laws of thermodynamics, the following formulas are introduced to calculate thermodynamic assessment indexes.

The heat transfer flow rate in the evaporator:

$$Q_{evaporator} = m_{wf}\left(h_4 - h_1\right) \tag{1}$$

The heat transfer flow rate in the condenser:

$$Q_{condenser} = m_{wf}\left(h_5 - h_7\right) \tag{2}$$

The consumed power of pump:

$$P_{pump} = m_{wf}\left(h_1 - h_7\right) \tag{3}$$

The turbine output shaft power:

$$P_{turbine} = m_{wf}\left(h_4 - h_5\right) \tag{4}$$

The net output power of TORC system:

$$P_{net} = P_{turbine} - P_{pump} \tag{5}$$

The specific net output power:

$$AP_{net} = P_{net} / m_{gw} \tag{6}$$

The thermal efficiency of TORC system:

$$\eta_t = P_{net} / Q_{evaporator} \times 100\% \tag{7}$$

Where m_{wf} and m_{gw} are the mass flow rate of working fluid and geothermal water, while h_i represents the specific state enthalpy with $i = 1...7$ as shown in Fig. 1.

The exergy of each state point:

$$E_i = m\left[\left(h_i - h_0\right) - T_0\left(s_i - s_0\right)\right] \tag{8}$$

Where m is the mass flow rate of objective fluid, while s_i represents the state point entropy with $i = 1...7$, and the subscript 0 implies the ambient condition.

The exergy losses of pump:

$$I_{pump} = m_{wf} T_0\left(s_1 - s_7\right) \tag{9}$$

The exergy losses of evaporator:

$$I_{evaporator} = \left(E_{gwin} + E_1\right) - \left(E_{gwout} + E_4\right) \tag{10}$$

The exergy losses of turbine:

$$I_{turbine} = m_{wf} T_0\left(s_5 - s_4\right) \tag{11}$$

The exergy losses of condenser:

$$I_{condenser} = \left(E_{cwin} + E_5\right) - \left(E_{cwout} + E_7\right) \tag{12}$$

The exergy losses caused by cooling water flows out:

$$I_{out}^{cooling\ water} = E_{cwout} - E_{cwin} \tag{13}$$

The total exergy losses of TORC system:

$$I_{system} = I_{pump} + I_{evaporator} + I_{turbine} + I_{condenser} + I_{out}^{cooling\ water} \tag{14}$$

The net exergy that geothermal water flows into system:

$$E_{in}^{gw} = P_{net} + I_{system} \tag{15}$$

The exergy efficiency of TORC system:

$$\eta_e = P_{net} / E_{in}^{gw} \tag{16}$$

The subscript *in* and *out* refers to the inlet and outlet state for objective fluid.

Before calculating the overall heat transfer coefficient and area of heat exchangers, the primary task is to identify the mass flow rate of working fluid. The inlet temperature (T_{gwin}) and mass flow rate of geothermal water (m_{gw}) are constant. Besides that, the minimal temperature difference is set larger than 10℃ between the evaporator inlet temperature of geothermal water and outlet temperature of working fluid.

First of all, referring to the Pinch Point Temperature Difference method, the evaporator outlet temperature of geothermal water (T_{gwout}) is assumed to get the outlet enthalpy (h_{gwout}) and calculate initial value of working fluid mass flow rate (m_{wf}):

$$m_{wf} = m_{gw}\left(h_{gwin} - h_{gwout}\right)\Big/\left(h_4 - h_1\right) \tag{17}$$

Secondly, the singe-phase flow region of geothermal water from gw_s to gw_{out} point is divided into one hundred segments as shown in Fig. 1. Thus the temperature difference of each segment can be determined. As a result, it could deduce the next state point temperature (T_{gwj}) from the beginning of T_{gws}.

$$T_{gwj} = T_{gws} - \left(T_{gws} - T_{gwout}\right)\Big/100\,j \tag{18}$$

The subscript j denotes the divided segments which range from 1 to 100.

Thirdly, based on the acquired variables of h_{gwj}, h_{gwout}, m_{wf}, the enthalpy (h_{gwj}) and temperature (T_{gwj}) of each state point for working fluids from 1 to 3 point can be obtained by using the first laws of thermodynamics.

$$h_{wfj} = h_1 + m_{gw}\left(h_{gwj} - h_{gwout}\right)\Big/m_{wf} \tag{19}$$

Lastly, the actual temperature difference between geothermal water and working fluids of each segment can be calculated. And the minimal temperature difference (ΔT_{act}) could be found out. Comparing it with 10℃, if the discrepancy satisfies the accuracy requirement (1%), it demonstrates that the assumed evaporator outlet temperature of geothermal water is reasonable. Otherwise, it needs to go back to the first step to presume another outlet temperature until meets the accuracy requirement.

2.2 Heat transfer model

The plate heat exchanger is selected as evaporator and condenser for its excellent heat transfer performance and compact structure. The geometric structure and dimension of plate heat exchanger are summarized in Table 3.

Table 3 Geometry of plate heat exchanger

Parameter	Value
Chevron angle, β (°)	60
Plate width, L_w (m)	0.65
Plate thickness, t (m)	0.0005
Corrugation pitch, Λ (m)	0.0085
Corrugation depth, b (m)	0.0025
Surface enlargement factor, ϕ	1.19
Hydraulic diameter, D_h (m)	0.0042
Equivalent diameter, D_{eq} (m)	0.005
Coefficient of thermal conductivity, λ_{PHE} (kW/(m·K))	0.0163

The heat transfer process in the evaporation and condenser are both divided into two sections. As illustrated above, the evaporator separates into single-phase flow and two-phase flow region according to the thermo-physical state of geothermal water. Similarly, the heat transfer area of condenser is divided into cooling and condensing region on the basis of the thermo-physical state of working fluid.

For the single-phase flow of geothermal water in the evaporator and cooling water in the condenser, the Leveque correlation [23] is used to calculate the heat transfer coefficient, which are α_{sgw} and α_{cw} respectively.

The Wang and Zhao correlation [24] is applied for calculation of geothermal water two-phase flow heat transfer coefficient (α_{tgw}) in the evaporator.

$$Nu = 0.00115\left(\mathrm{Re}_l / H\right)^{0.983} \mathrm{Pr}_l^{0.33} \left(\rho_l / \rho_v\right)^{0.248} \tag{20}$$

$$\alpha_{tgw} = Nu\lambda_l / D_{eq} \tag{21}$$

$$\mathrm{Re}_l = G_{gw}\left(1 - x_0\right) D_{eq} / \mu_l \tag{22}$$

$$\mathrm{Pr}_l = c_{p,l}\mu_l / \lambda_l \tag{23}$$

$$H = c_{p,l}\left(T_{ave} - T_{wall}\right) \Big/ \left(i_{fg} + 0.68 c_{p,l}\left(T_{ave} - T_{wall}\right)\right) \tag{24}$$

Where the indicators with subscript l are calculated based on the mean temperature of steam and wall temperature (T_{ave}), and the indicators with subscript v are calculated based on the average steam temperature, λ represents the thermal conductivity of objective water, G_{gw} implies the total mass flux of geothermal water, x_0 is the vapor quality at the end state of two-phase flow region which sets as 0, D_{eq} is the equivalent diameter of plate heat exchanger, and i_{fg} represents the latent heat of water from liquid to vapor state.

As for the tans-critical working fluids in evaporator, Jackson correlation [25] is adopted to calculate the heat transfer coefficient ($\alpha_{tc,\,wf}$).

$$Nu = 0.0183\,\mathrm{Re}^{0.82}\,\mathrm{Pr}^{0.5}\left(\rho_{wall}/\rho\right)^{0.3}\left(\overline{c_p}/c_p\right)^{n} \tag{25}$$

$$\alpha_{tc,\,wf} = Nu\lambda/D_h \tag{26}$$

$$\overline{c_p} = \left(h_{wall} - h_c\right)/\left(T_{wall} - T_c\right) \tag{27}$$

$$\mathrm{Re} = \rho v D_h/\mu \tag{28}$$

$$\mathrm{Pr} = c_p\mu/\lambda \tag{29}$$

$$\begin{aligned} &n = 0.4,\ T_c < T_{wall} < T_{cri},\ 1.2T_{cri} < T_c < T_{wall} \\ &n = 0.4 + 0.2\left[\left(T_{wall}/T_{cri}\right) - 1\right],\ T_c < T_{cri} < T_{wall} \\ &n = 0.4 + 0.2\left[\left(T_{wall}/T_{cri}\right) - 1\right]\left[1 - 5\left(T_c/T_{cri} - 1\right)\right],\ T_{cri} < T_c < 1.2T_{cri},\ T_c < T_{wall} \end{aligned} \tag{30}$$

Where T_c is the characteristic temperature of working fluid and h_c is obtained based on it. Additionally, other indexes like ρ_{wall} and h_{wall} are acquired under the condition of plate heat exchanger wall-side temperature (T_{wall}), T_{cri} is the critical temperature of working fluid, and D_h is hydraulic diameter which calculated by $D_h = 2b/\phi$.

For the cooling part in the condenser, the Chisholm correlation [26] is employed for calculating the working fluid heat transfer coefficient (α_{swf}).

For the condensing part in the condenser, the Kandlikar correlation [27] is used to calculate the working fluid heat transfer coefficient (α_{twf}).

$$\alpha_l = 0.2092\left(\lambda_l / D_h\right)\mathrm{Re}_l^{0.78}\,\mathrm{Pr}_l^{0.33}\left(\mu/\mu_{wall}\right)^{0.14} \tag{31}$$

$$\mathrm{Re}_l = G_{wf}\,D_h/\mu_l \tag{32}$$

$$\mathrm{Pr}_l = c_{p,l}\,\mu_l/\lambda_l \tag{33}$$

$$Co = \left(\rho_v/\rho_l\right)\left(1/x_m - 1\right)^{0.8} \tag{34}$$

$$Fr_l = G_{wf}^2 \Big/ \left(\rho_l^2 g D_h\right) \tag{35}$$

$$Bo = q/G_{wf} i_{fg} \tag{36}$$

$$\alpha_{twf} = \alpha_l\left(0.25Co^{-0.45}Fr_l^{0.25} + 75Bo^{0.75}\right) \tag{37}$$

Where g implies the acceleration of gravity which is 9.8(m/s^2), G_{wf} is the total mass flow rate of working fluid, and x_m is the vapor quality which sets 0.5.

After acknowledging the heat transfer coefficient of each section, the heat exchanger areas (A) are derived from the following equations.

$$A = Q/U/\Delta T_m \tag{38}$$

$$1/U = 1/\alpha_{hot-side} + t/\lambda_{PHE} + 1/\alpha_{cold-side} \tag{39}$$

Where Q is the heat transfer mass flow and U is the overall heat transfer coefficient of each part, while ΔT_m is the log mean temperature difference between hot-side and cold-side and λ_{PHE} is the thermal conductivity of plate heat exchanger.

2.3 Techno-economic model

For the purpose of giving an all-around viewpoint on the techno-economic properties of the ORC system, six parameters are collected that covered two aspects of investment and expected return. In detail, which are heat transfer area per net output power (APR), turbine characteristic size parameters (SP), gross cost based on the latest economic indexes ($\mathrm{Cos}t_{2019}$), electricity production cost (EPC), depreciated payback period (DPP) and saving to investment ratio (SIR).

The APR is employed as evaluation criterion of the heat exchanger compactness, the more compact of the heat exchanger structure, the smaller the APR and the lower the initial investment, which is defined as:

$$APR = \left(A_e + A_c\right) / P_{net} \tag{40}$$

The SP is regarded as an indicator of the relative cost of TORC system by measuring the size of turbine, which is defined as:

$$SP = \sqrt{V_5} / \Delta h_{isen}^{0.25} \tag{41}$$

Where V_5 is the volume flow of turbine outlet (state point 5) while Δh_{isen} is isentropic enthalpy drop before and after expansion (state point 4 to 5).

The $\mathrm{Cos}t_{2019}$ is determined based on the Module Cost Technique [28], It represents the sum of bare module costs of the main components in ORC system, which is given below:

$$\mathrm{Cos}t_{2001} = \mathrm{C}_{BM,\,pump} + \mathrm{C}_{BM,\,evaporator} + \mathrm{C}_{BM,\,turbine} + \mathrm{C}_{BM,\,condenser} \tag{42}$$

$$\mathrm{Cos}t_{2019} = \mathrm{Cos}t_{2001} CEPCI_{2019} / CEPCI_{2001} \tag{43}$$

Where $CEPCI$ is the chemical engineering plant cost index while $CEPCI_{2001} = 397$ and $CEPCI_{2019} = 607.5$ [29].

As presented in Table 4, the bare module cost (C_{BM}) is defined as the product of purchased cost (C_p) and bare module cost factor (F_{BM}). C_p is related to the capacities ($P_{pump}, P_{turbine}$) and size parameters (A_e, A_c) of each component which are acquired from the optimal results. F_{BM} considers the material factor (F_M) and pressure factor (F_P). The materials for heat exchangers and pump are stainless steel and the pump type is centrifugal. Then, the coefficients like B, C, K could be determined by the arranged configurations.

Table 4 Main components bare module cost equations

Component	Bare module cost equation	Coefficient				
		$K_1/K_2/K_3$	$C_1/C_2/C_3$	B_1/B_2	F_M	F_{BM}
Turbine	$C_{BM,turbine} = C_{p,turbine} F_{BM,turbine}$ $\lg C_{p,turbine} = K_{1,t} + K_{2,t} \lg P_t + K_{3,t} (\lg P_t)^2$	$K_{1,t} = 2.626$ $K_{2,t} = 1.440$ $K_{3,t} = -0.178$	/	/	/	3.5
Pump	$C_{BM,pump} = C_{p,pump} F_{BM,pump}$ $\lg C_{p,pump} = K_{1,p} + K_{2,p} \lg P_p + K_{3,p} (\lg P_p)^2$ $F_{BM,pump} = B_{1,p} + B_{2,p} F_{M,pump} F_{P,pump}$ $\lg F_{p,pump} = C_{1,p} + C_{2,p} \lg P_P + C_{3,p} (\lg P_p)^2$	$K_{1,p} = 3.389$ $K_{2,p} = 0.054$ $K_{3,p} = 0.155$	$C_{1,p} = -0.394$ $C_{2,p} = 0.396$ $C_{3,p} = -0.002$	$B_{1,p} = 1.89$ $B_{2,p} = 1.35$	2.32	/
Evaporator	$C_{BM,evaporator} = C_{p,evapoeator} F_{BM,evaporator}$ $\lg C_{p,evaporator} = K_{1,e} + K_{2,e} \lg A_e + K_{3,e} (\lg A_e)^2$ $F_{BM,evaporator} = B_{1,e} + B_{2,e} F_{M,evaporator}$	$K_{1,e} = 4.666$ $K_{2,e} = -0.156$ $K_{3,e} = 0.155$	/	$B_{1,e} = 0.96$ $B_{2,e} = 1.21$	2.45	/
Condenser	$C_{BM,condenser} = C_{p,condenser} F_{BM,condenser}$ $\lg C_{p,condenser} = K_{1,c} + K_{2,c} \lg A_c + K_{3,c} (\lg A_c)^2$ $F_{BM,condenser} = B_{1,c} + B_{2,c} F_{M,condenser}$	$K_{1,c} = 4.666$ $K_{2,c} = -0.156$ $K_{3,c} = 0.155$	/	$B_{1,c} = 0.96$ $B_{2,c} = 1.21$	2.45	/

The EPC demonstrates the relative scales of capital input and output from the perspectives of per unit power generation cost, which is presented as:

$$EPC = \left(\mathrm{Cost}_{2019} CRF + f_k \,\mathrm{Cost}_{2019}\right) \Big/ \left(P_{net} h_{working-time}\right) \tag{44}$$

$$CRF = i(1+i)^{time} \Big/ \left((1+i)^{time} - 1\right) \tag{45}$$

Where CRF is the capital recovery factor, f_k is operation and maintenance factor which sets as 1.65%, $h_{working-time}$ is the working time of each year which assumes to be 8100h, i is the annual interest which regarded as 5% and $time$ is the life cycle assessment time of 15 years.

The DPP gives a clearly projected investment return time of the ORC system, which is defined as:

$$DPP = -\ln\left(1 - k\,\mathrm{Cost}_{2019} / F_{n0}\right) / \ln(1+k) \tag{46}$$

$$F_{n0} = E_P \left(P_{net} h_{working-time}\right) - f_k \,\mathrm{Cost}_{2019} \tag{47}$$

Where k implies the depreciated ratio which is 5%, F_{n0} is the system net income and E_P is the electricity sale price which sets as 0.1($/kW·h) [30]. Moreover, the net output power (P_{net}) is completely regarded as net electricity generation as result that the power generation efficiency sets as 1.

The SIR figures out the proportion of the predicted profit and initial investment, which is defined as:

$$SIR = B_{time} / C_{time} \tag{48}$$

$$B_{time} = \sum_{j=1}^{time} \left(P_{net} h_{working-time} E_p (1+r)^j \Big/ (1+i)^j\right) \tag{49}$$

$$C_{time} = \sum_{j=0}^{time} \left(\left(f_k \,\mathrm{Cost}_{2019}\right)(1+r)^j \Big/ (1+i)^j\right) \tag{50}$$

Where B_{time} and C_{time} are the net value of total income and investment during the period of life cycle assessment time which $j = 1...15$, r is the inflation rate which sets as 2.9%.

2.4 Three-level fuzzy decision model

In the paper, the three-level fuzzy decision model is established based on the properties model of working fluids, the thermodynamic model and the techno-economic model as put forward earlier, which are regarded as the first, second and third level respectively. The development and programming of the method is accomplished by the following four steps:

Step (1) - Acquiring the optimal results of decision criteria by choosing appropriate indicator as the objective function according to the realistic operation requirements.

Step (2) - A pair-wise comparison matrix of each decision criterion for schemes is constructed so as to rank in sequence and assign the semantic score. After the normalization of semantic score, the weighting set of each criterion could be obtained.

Step (3) - Similar to step two, a pair-wise comparison matrix of each decision criterion for three classified levels is built, the weighting set calculation is subject to the relative importance of decision criteria within each level.

Step (4) - After acknowledging the weighting set of each criterion, the weighting matrix for schemes ($\boldsymbol{R}_i$) and levels ($\boldsymbol{W}_i$) can be developed. And the evaluation set ($\boldsymbol{B}_i$) can be calculated by the following equation:

$$\boldsymbol{B}_i = \boldsymbol{W}_i \times \boldsymbol{R}_i \tag{51}$$

For the second level, evaluation result of the first level should be inserted into the $\boldsymbol{R}_i$ as the last row. The original $\boldsymbol{W}_i$ of second level needs to multiply $n/(n+1)$ if n decision criteria are included. Next, a new $\boldsymbol{W}_i$ has to be formed by assigning $1/(n+1)$ in the final position of the former one. For the third level, the same procedure is undergoing repeatedly to gain $\boldsymbol{B}_i$.

Summarizing the three mathematical models above, Fig. 3 gives a clear flow chart of the construction procedures.

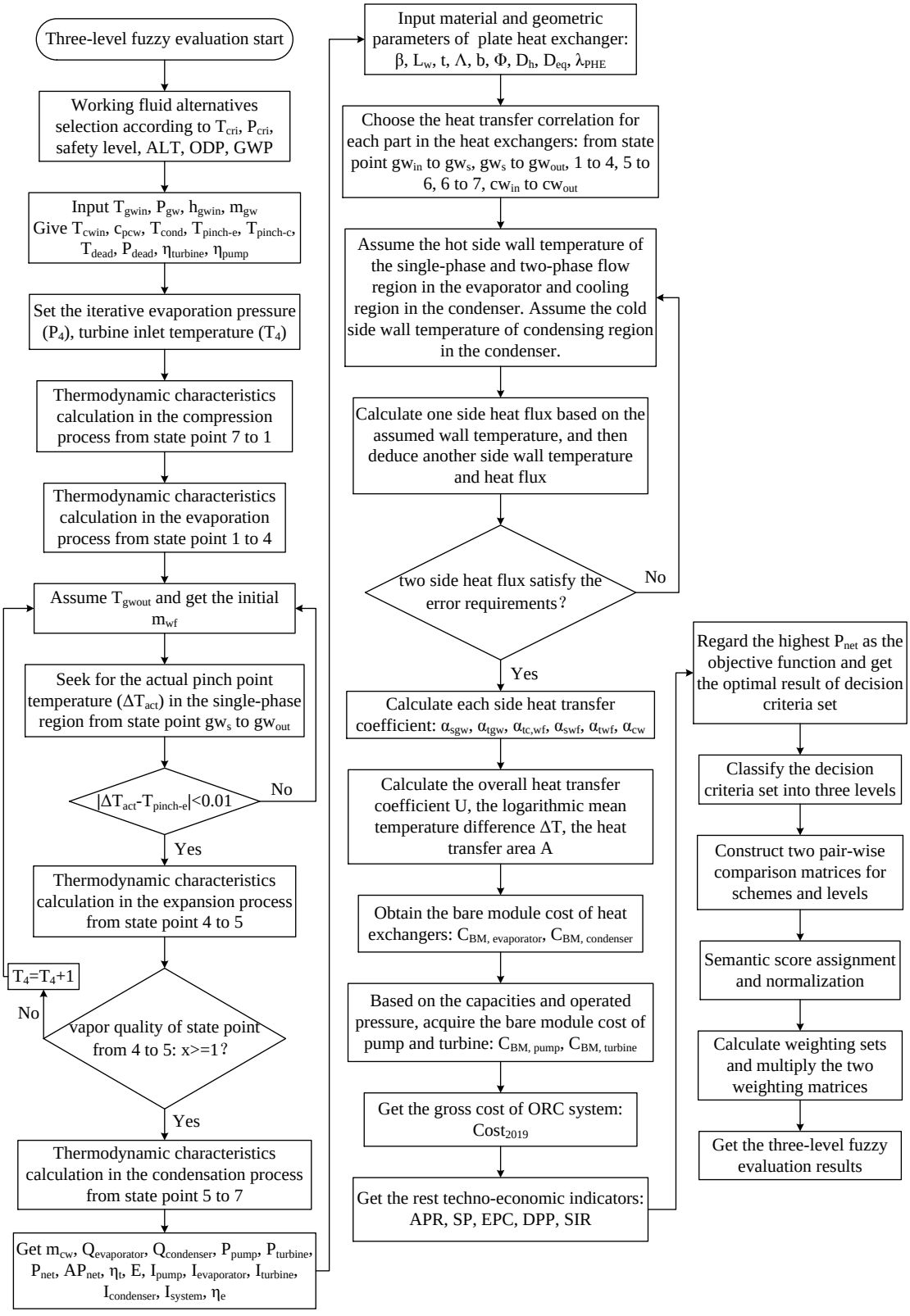

Fig. 3. The three-level fuzzy evaluation procedures

3 Results and discussion

3.1 Thermodynamic performance

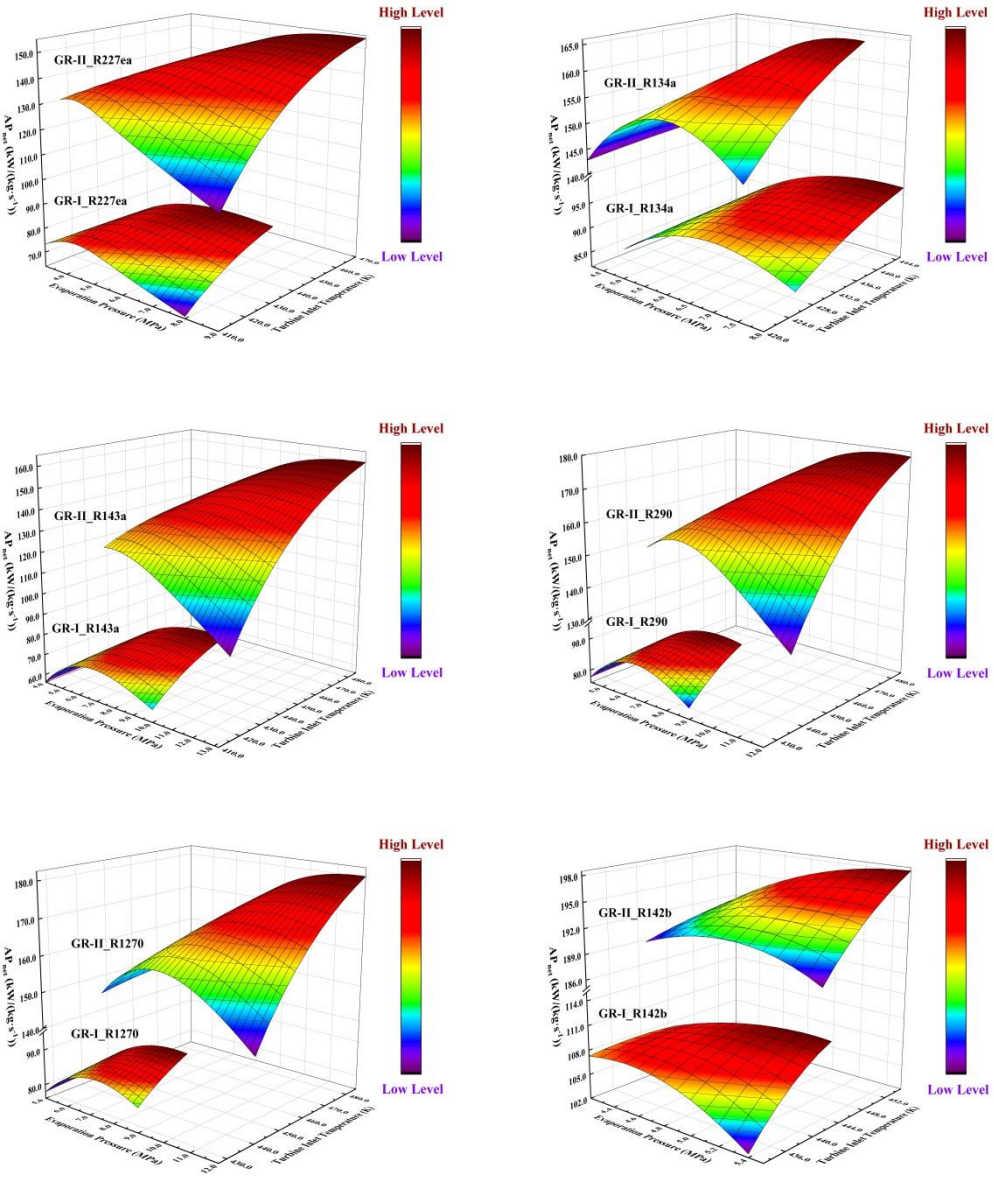

Fig. 4. Specific net output power (AP_{net}) variation in two geothermal reservoirs

In this study, the specific net output power (AP_{net}), thermal efficiency (η_t) and exergy efficiency (η_e) are determined to estimate the thermodynamic performance of the TORC system designed for both geothermal reservoirs (GR-I and GR-II). As shown in Figs. 4, 5 and 6, the overall variation of the three indexes shows both similarities and diversities with increasing evaporation pressure (P_4) and turbine inlet temperature (T_4) for each working fluid in two different geothermal reservoirs. Moreover, Fig. 4 indicates AP_{net} of the six selected working fluids in GR-II which ranges from 93.73-198.14kW/(kg·s^{-1}) is apparently higher than that of GR-I which is from 56.46-110.94kW/(kg·s^{-1}), indicting a higher power capacity of GR-II. Besides, Fig. 4 demonstrates AP_{net} increases firstly and then decreases when raising P_4 under given T_4. It is because turbine output shaft power ($P_{turbine}$) enhances obviously while P_4 increases from lower values (but still exceed the critical pressure of the working fluid). And the consumed power of pump (P_{pump}) increases more rapidly than $P_{turbine}$ with further increase of P_4, which results that the upward trend of AP_{net} gradually slows down until it starts deceasing. In addition, due to the limits of pinch point temperature difference ($T_{pinch-e}$) and decomposition temperature (T_{de}) of working fluids, AP_{net} keeps increasing while T_4 grows up to reach the maximal value under higher P_4. Furthermore, AP_{net} shows upward tendency firstly and then goes downward when given a lower P_4. Comparing the optimal results of working fluids in GR-I, R142b is able to acquire the largest AP_{net} of 110.94kW/(kg·s^{-1}) at the condition that the P_4 is 5.2MPa and T_4 is 445K. On the contrary, R143a obtains smallest AP_{net} of 81.77kW/(kg·s^{-1}) in the case of the

460 P_4 is 9.4MPa and T_4 is 445K. With regard to GR-II, R142b maintains the highest

461 AP_{net} as well, which is 198.14kW/(kg·s^{-1}) when the P_4 is 5.5MPa and T_4 is

462 455K. And R227ea yields lowest AP_{net} of 154.02kW/(kg·s^{-1}), for the P_4 is

463 8.6MPa and T_4 is 470K.

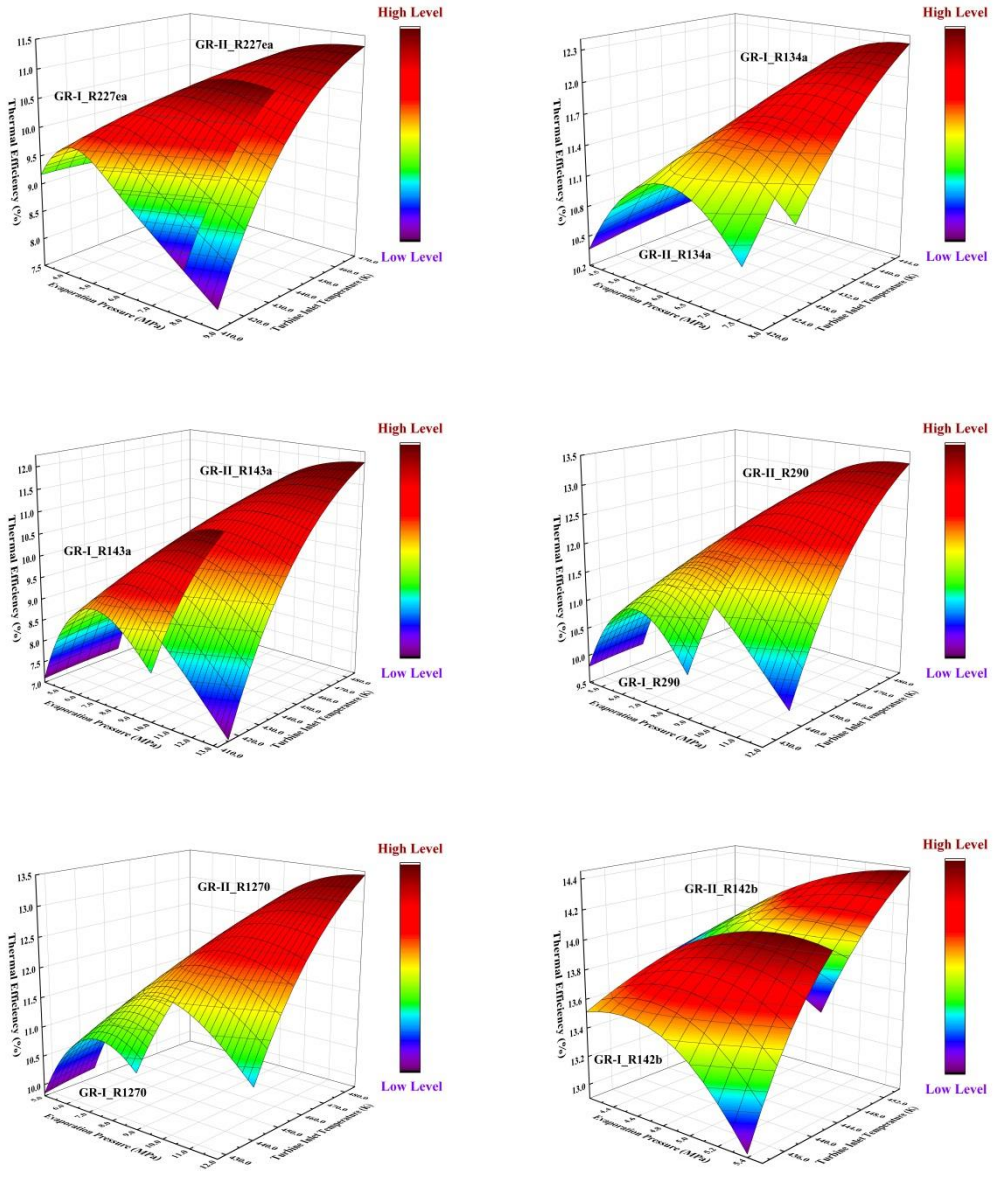

Fig. 5. Thermal efficiency (η_t) variation in two geothermal reservoirs

Thermal efficiency (η_t) is defined as the ratio of net power output (P_{net}) to the amount of heat absorbed during the evaporation process, as shown in Eq. (7). The change of η_t by varying evaporation pressure (P_4) and turbine inlet temperature (T_4) is illustrated in Fig. 5. As far as the η_t of each working fluid is concerned, there exists regions that are partially overlapped between GR-I and GR-II, which ranges from 7.10-14.05% and 7.04-14.43%, indicating that even though geothermal reservoirs have different power capacities, they could have similar energy conversion efficiency ranges applying TORC. Specifically, it is observed that η_t of all selected working fluids can be described as increasing and dropping later with an increase of P_4 under investigated T_4. The alteration of η_t is similar with AP_{net}. For this reason, the η_t rises faster at lower P_4 and stabilizes till it decreases as P_4 increases further. Additionally, with the restrictions of $T_{pinch-e}$ and T_{de}, η_t represents an inclination of rising up continuously with increasing T_4 to the maximum under higher P_4. The reason can be explained from that, although the enthalpy difference ($h_4 - h_5$) becomes larger and the mass flow rate of working fluids (m_{wf}) is declining in the course of expansion, the turbine output shaft power ($P_{turbine}$) still increases and the pump power consumption (P_{pump}) decreases as T_4 continues increasing. In the meanwhile, when the system operates at a lower P_4, η_t behaves in a trend of increasing first and then diminishes as T_4 grows up. The maximum results of η_t for working fluids in GR-I and GR-II are both R142b which are 14.05% and 14.43% respectively, for the P_4 and T_4 are 5.1MPa, 445K and 5.5MPa, 455K. To the opposite, R143a and R227ea have the minimal η_t in GR-I and GR-II with

the values of 10.66% and 11.32%.

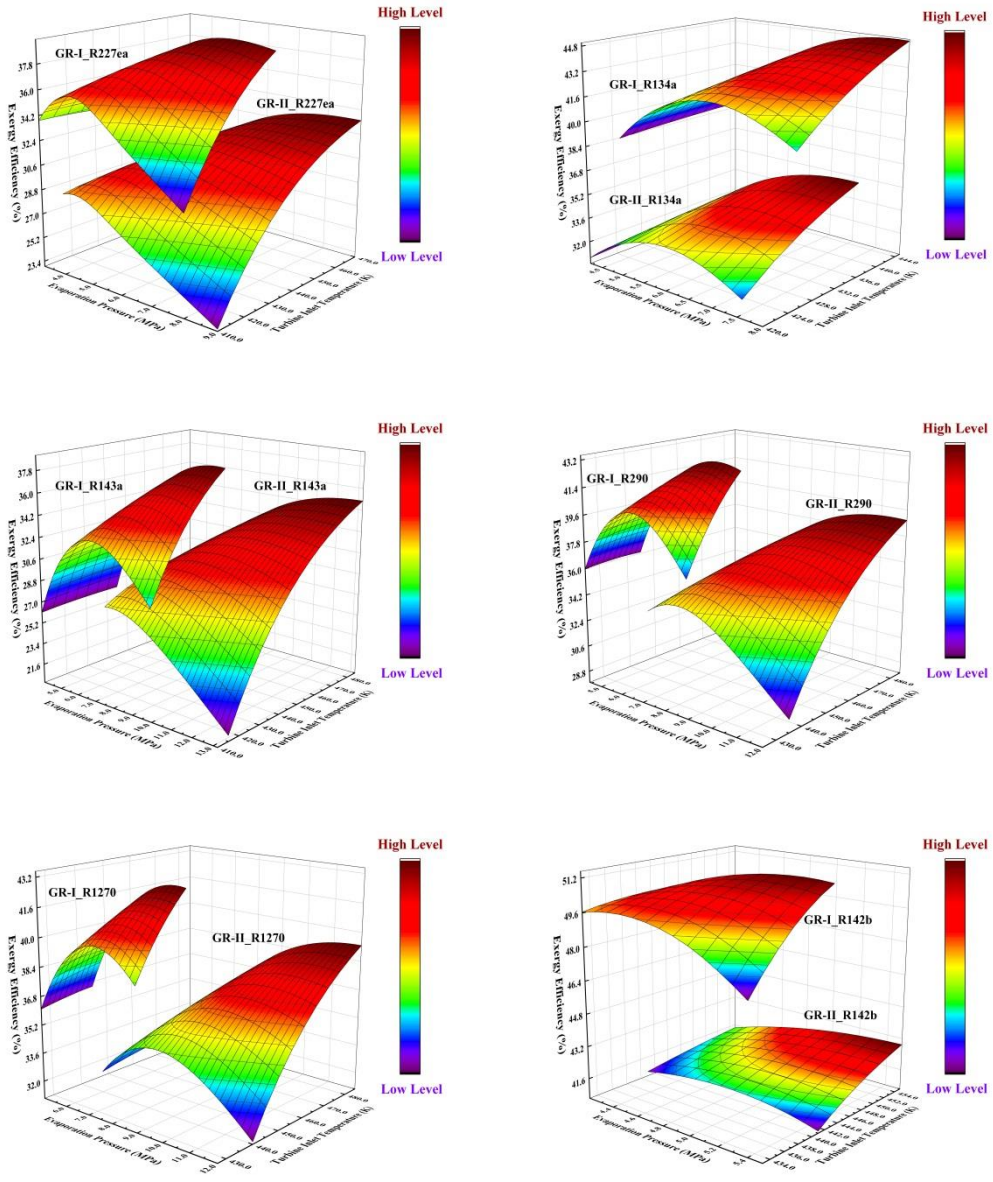

Fig. 6. Exergy efficiency (η_e) variation in two geothermal reservoirs

Exergy signifies the greatest beneficial output power that geothermal system possesses. The exergy efficiency (η_e) is employed for assessing the exergy utilization, which is characterized as the ratio of net output power (P_{net}) to the net exergy flows into the system (E_{in}^{gw}), as given in Eq. (16). Typically, it can be noticed from Fig. 6 that the η_e in GR-I is normally higher than GR-II. The ranges are 26.11-51.42% for GR-I and 23.14-42.89% for GR-II, which indicates that although GR-I has smaller power capacity, the exergy is fully utilized compared to GR-II. Particularly, Fig. 6 denotes that the arc-surface changing trend of η_e is familiar with that of AP_{net} and η_t. Increasing of η_e is owing to the thermal matching performance becomes better between heat sources and working fluids and the exergy loss (I_{system}) reduces constantly with an increment of lower evaporation pressure (P_4). Instead, the reduction of P_{net} is more markedly than the I_{system} decreases with further increase of P_4, leading to the downward tendency for η_e. What's more, the η_e shows a trend of growing up for that P_{net} keeps increasing while I_{system} turns into dropping by improving turbine inlet temperature (T_4) under investigated P_4. According to optimal results of the working fluids, R142b achieves the biggest η_e of 51.42% and 42.90% in the GR-I and GR-II, with the P_4 and T_4 are 5.2MPa, 445K and 5.5MPa, 455K. And R143a and R227ea get lowest exergy efficiency of 38.30% and 33.42% for the two geothermal reservoirs.

3.2 Techno-economic performance

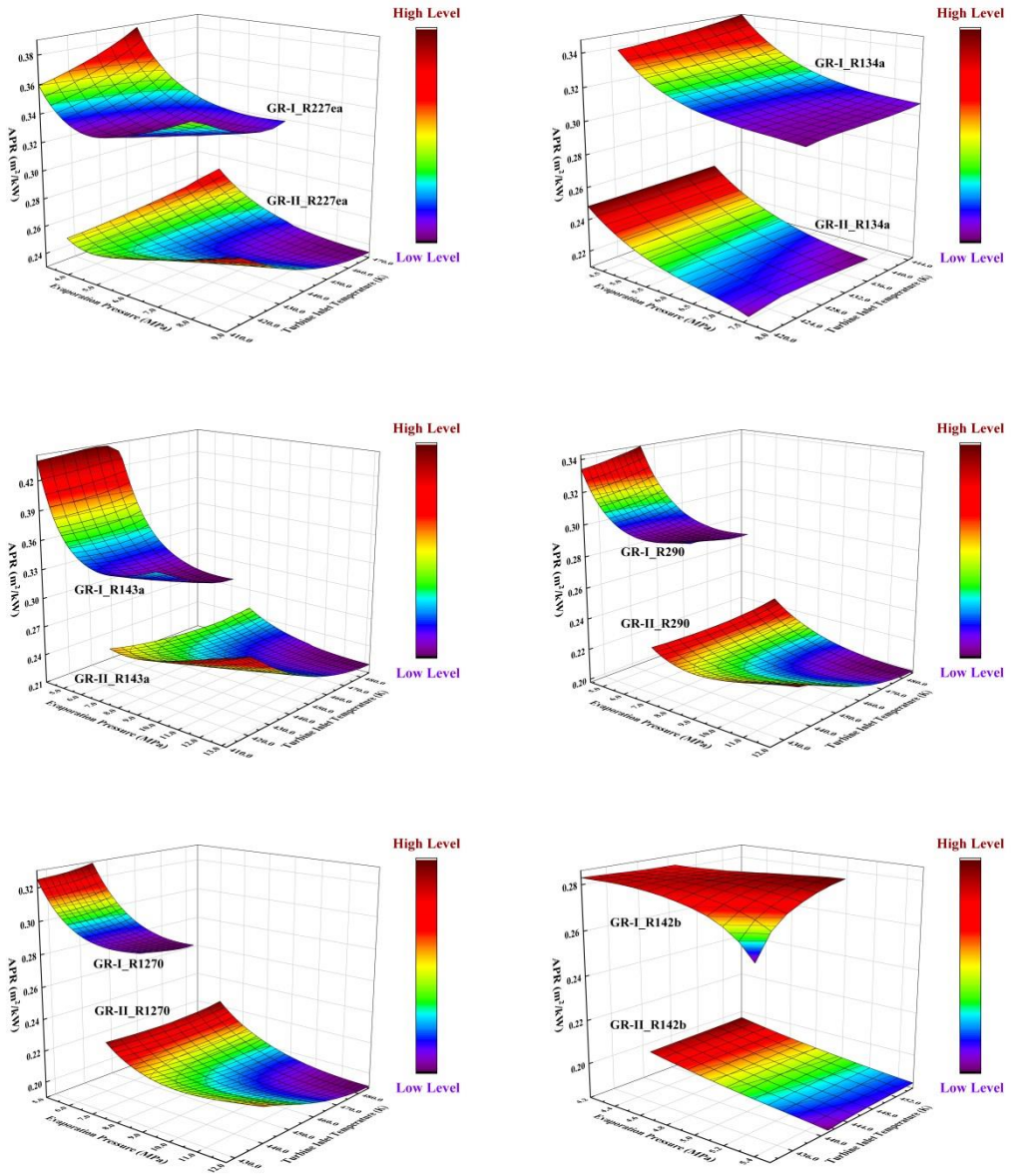

Fig. 7. Heat transfer area per net output power (APR) variation in two geothermal reservoirs

Utilizing the techno-economic evaluation model established previously, the heat transfer area per net output power (APR) and electricity production cost (EPC) are adopted for detailed illustration of the techno-economic properties of TORC system. First of all, as depicted in Figs. 7 and 8, the map alteration of two indexes for each working fluid (expect R142b) expresses consistent changing trend under the influence of evaporation pressure (P_4) and turbine inlet temperature (T_4) in the both two geothermal reservoirs. The APR and EPC values in GR-I is commonly above those of GR-II. As for GR-I and GR-II, APR ranges from 0.262-0.444(m^2/kW) and 0.185-0.290(m^2/kW). EPC ranges from 0.030-0.054($/(kW·h)) and 0.022-0.055 ($/(kW·h)), indicating that GR-II is more profitable in the techno-economic perspective. Furthermore, APR implies the compactness of heat exchangers structure which refers to the ratio of hear transfer areas of all heat exchangers to net output power. For the purpose of cutting down the overall cost of the whole system, it's better to achieve the APR as low as possible. Then, it can be seen form Fig. 7 that APR of R227ea, R143a, R290 and R1270 decreases initially before increasing in both two geothermal reservoirs when increasing P_4 under given T_4. Since the net output power (P_{net}) first increases and then decreases for the four working fluids with which trend of variation is more dramatically than the heat transfer areas change. Regarding the APR of R134a and R142b, it's decreasing yet with an increment of P_4 under given T_4. The difference of R134a and R142b from other four alternatives accounts for the downward trend of heat transfer areas varies more significantly than that of P_{net}. Moreover, the region of minimum APR for the

working fluids (expect R142b in GR-I) begins to appear when further increasing P_4 and T_4 simultaneously. Summarily, concluding from the optimal results under the operated conditions. R142b acquires the lowest APR of 0.262(m^2/kW) and 0.185(m^2/kW) in GR-I and GR-II, for 5.4MPa, 433K and 5.5MPa, 441K of the P_4 and T_4. Additionally, R227ea obtains higher APR of 0.331(m^2/kW) and 0.234(m^2/kW) respectively, for 5.8MPa, 425K and 9.0MPa, 470K.

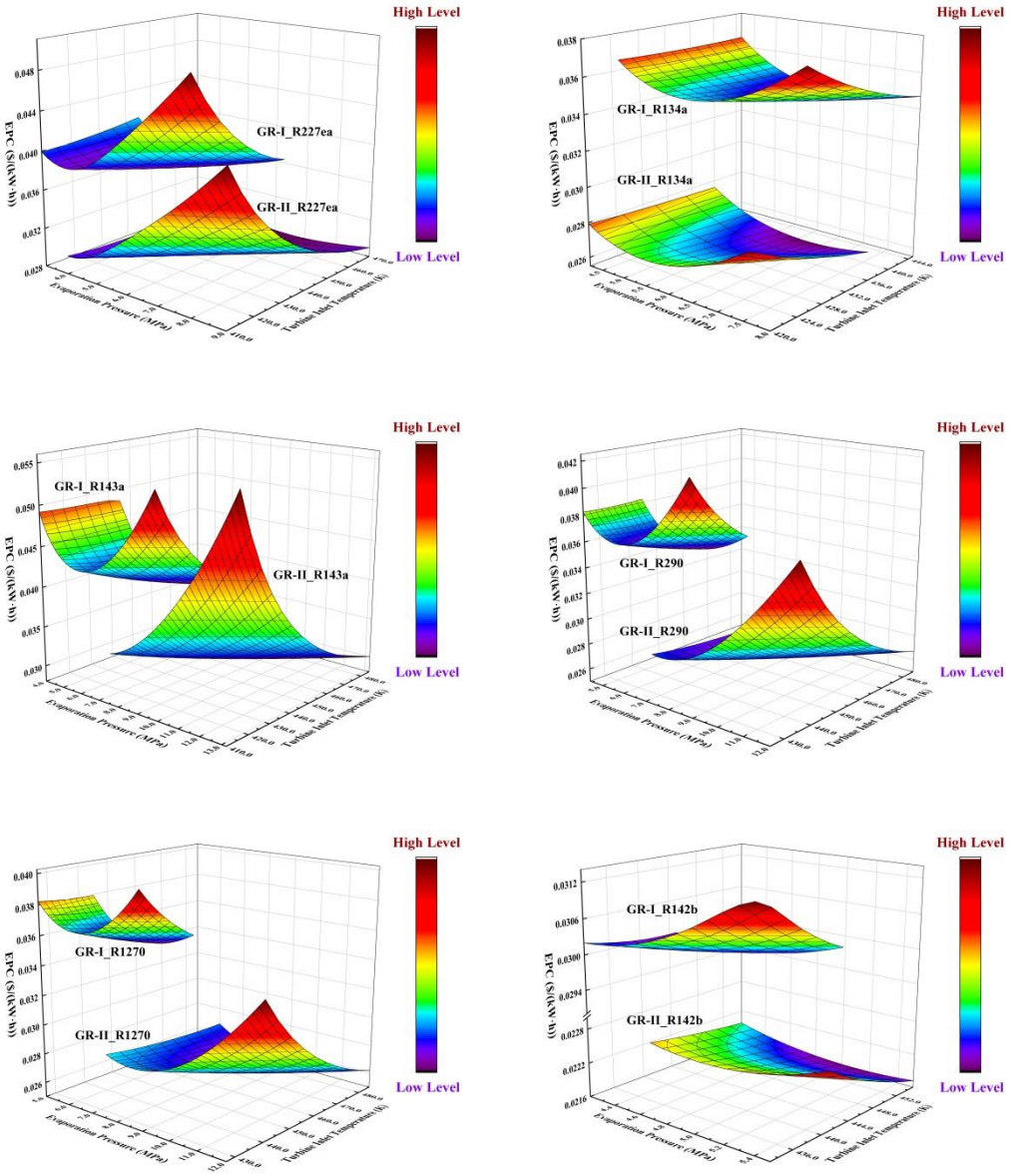

Fig. 8. Electricity production cost (EPC) variation in two geothermal reservoirs

EPC is directly proportional to the gross cost ($Cost_{2019}$) and inversely to the net output power (P_{net}) and the whole working time ($h_{working-time}$) of the TORC system. Hence, in the case of a certain $h_{working-time}$ with increasing the evaporation pressure (P_4) under given turbine inlet temperature (T_4), Fig. 8 shows that EPC exhibits a trend of decrease initially and increase afterwards for the reason that P_{net} increases first and then decreases, meanwhile, the pressure tolerance of components is required to enhance which leads to an inevitable increase in $Cost_{2019}$. Similarly, the EPC decreases firstly and then increases when increasing T_4 under lower P_4. The explanation for this variation is similar with ranging P_4 but the discrepancy exists that overall heat transfer areas keep increasing which draws an increase in $Cost_{2019}$. When considering the limits of the maximal T_4 under higher P_4, the upward tendency of EPC would not appear anymore. By comparing the optimal results between working fluids, the lowest EPC appears at R142b of 0.030($/(kW·h)) and 0.022($/(kW·h)) when the P_4 and T_4 are 4.6MPa, 445K and 5.1MPa, 455K in GR-I and GR-II. Moreover, R143a gets higher EPC of 0.040($/(kW·h)) and 0.0285($/(kW·h)) for 7.6MPa, 445K and 9.4MPa, 485K of P_4 and T_4.

3.3 Three-level fuzzy evaluation

As illustrated in maps of thermodynamic and techno-economic parameters above, the iteration outcomes can be exported by varying the tested evaporation pressure (P_4) and turbine inlet temperature (T_4) for each working fluid alternative. In the meantime, the case study regards the maximal P_{net} as objective function to obtain the optimal results for GR-I and GR-II. As listed in Tables 5 and 6, the values of the rest indexes such as η_t or APR are acknowledged under the same values of P_4 and T_4 when P_{net} gets the maximum. In this paper, the available options of scheme included R227ea (D1), R134a (D2), R143a (D3), R290 (D4), R1270 (D5) and R142b (D6). The decision criteria set is comprised of Safety Level (C1), ALT (C2), ODP (C3), GWP (C4), P_{net} (C5), η_t (C6), η_e (C7), APR (C8), SP (C9), $\mathrm{Cos}t_{2019}$ (C10), EPC (C11), DPP (C12) and SIR (C13).

Judging by the rules of criteria for higher-the-better such as C5, C6, C7 and C12 or lower-the-better involving C1, C2, C3, C4, C8, C9, C10, C11 and C13, a pair-wise comparison matrix of the P_{net} (C5) for schemes in GR-I is constructed for instance. As depicted in Table 7, it can be seen that the values on diagonal line are all 0.5 in the matrix on account of the P_{net} of each scheme is identical to itself. When it comes to comparing the P_{net} of D1 to D2, the result is 0, because of the value of P_{net} in D1 is lower than D2. Conversely, 1 is appeared when comparing D2 with D1 for the P_{net} of D2 is higher than D1. The sum of each row is got after the consistence checking between all the schemes. Arranging the sum of schemes in a descending order, those are D6, D2, D4, D5, D1 and D3. Furthermore, since the ranking is based on an interval of 0.5, D6 acquires the highest of 5.5 at the first position and the semantic score is assigned 1. D2 obtains 4.5 and scored 0.818 in the third place. The weighting is calculated by means of the semantic score for each scheme dividing the sum semantic scores for all schemes in the normalization process. Then, the weighting set for other twelve criteria are derived from the same procedures. Tables 8 and 9 list the results of weighting matrix for all schemes ($\boldsymbol{R}_i$) after normalization in GR-I and GR-II.

Table 5 Simulated optimal results of GR-I

Working Fluid	P_4 /MPa	T_4 /K	P_{net} /kW	η_t /%	η_e /%	APR(m^2/kW)	SP/m	$Cost_{2019}$ (10^5\$)	EPC(\$/(kW·h))	DPP/Year	SIR	Scheme
R227ea	6.6	445	1158.13	10.78	39.40	0.338	0.068	31.84	0.038	4.062	3.115	D1
R134a	7.6	445	1318.65	12.31	44.91	0.308	0.064	32.59	0.034	3.589	3.466	D2
R143a	9.4	445	1115.41	10.64	38.29	0.325	0.052	32.69	0.041	4.380	2.923	D3
R290	7.6	445	1265.92	11.93	43.25	0.298	0.070	32.62	0.036	3.766	3.324	D4
R1270	8.6	445	1256.59	11.90	43.00	0.291	0.064	32.58	0.036	3.794	3.303	D5
R142b	5.2	445	1513.27	14.04	51.42	0.285	0.087	32.74	0.030	3.084	3.959	D6

Table 6 Simulated optimal results of GR-II

Working Fluid	P_4 /MPa	T_4 /K	P_{net} /kW	η_t /%	η_e /%	APR(m^2/kW)	SP/m	$Cost_{2019}$ (10^5\$)	EPC(\$/(kW·h))	DPP/Year	SIR	Scheme
R227ea	8.6	470	1694.22	11.31	33.42	0.234	0.067	34.94	0.029	2.923	4.153	D1
R134a	7.4	440	1821.87	12.12	35.90	0.214	0.064	34.08	0.026	2.621	4.578	D2
R143a	13	485	1760.56	12.01	34.96	0.219	0.051	37.82	0.030	3.060	3.988	D3
R290	11.2	485	1966.04	13.28	38.92	0.199	0.068	36.98	0.026	2.637	4.554	D4
R1270	11.8	485	1981.99	13.43	39.28	0.191	0.063	37.14	0.026	2.626	4.571	D5
R142b	5.5	455	2179.54	14.43	42.89	0.187	0.087	33.98	0.022	2.146	5.494	D6

Table 7 Consistence checking, semantic score assignment and weighting calculation of net output power (P_{net}) for scheme

C5	D1	D2	D3	D4	D5	D6	Sum	Score	Weighting
D1	0.5	0	1	0	0	0	1.5	0.429	0.1133
D2	1	0.5	1	1	1	0	4.5	0.818	0.2161
D3	0	0	0.5	0	0	0	0.5	0.333	0.088
D4	1	0	1	0.5	1	0	3.5	0.667	0.1762
D5	1	0	1	0	0.5	0	2.5	0.538	0.1422
D6	1	1	1	1	1	0.5	5.5	1	0.2642

Table 8 Weighting of decision criteria for each scheme after normalization of semantic score in GR-I

	C1	C2	C3	C4	C5	C6	C7	C8	C9	C10	C11	C12	C13
D1	0.2383	0.1133	0.1806	0.1133	0.1133	0.1133	0.1133	0.088	0.1422	0.2642	0.1133	0.1133	0.1133
D2	0.2383	0.1762	0.1806	0.1762	0.2161	0.2161	0.2161	0.1422	0.2161	0.1762	0.2161	0.2161	0.2161
D3	0.1429	0.088	0.1806	0.088	0.088	0.088	0.088	0.1133	0.2642	0.1133	0.088	0.088	0.088
D4	0.1022	0.2161	0.1806	0.2161	0.1762	0.1762	0.1762	0.1762	0.1133	0.1422	0.1762	0.1762	0.1762
D5	0.1022	0.2642	0.1806	0.2642	0.1422	0.1422	0.1422	0.2161	0.1762	0.2161	0.1422	0.1422	0.1422
D6	0.1761	0.1422	0.097	0.1422	0.2642	0.2642	0.2642	0.2642	0.088	0.088	0.2642	0.2642	0.2642

Table 9 Weighting of decision criteria for each scheme after normalization of semantic score in GR-II

	C1	C2	C3	C4	C5	C6	C7	C8	C9	C10	C11	C12	C13
D1	0.2383	0.1133	0.1806	0.1133	0.088	0.088	0.088	0.088	0.1422	0.1762	0.1133	0.1133	0.1133
D2	0.2383	0.1762	0.1806	0.1762	0.1422	0.1422	0.1422	0.1422	0.1762	0.2161	0.2161	0.2161	0.2161
D3	0.1429	0.088	0.1806	0.088	0.1133	0.1133	0.1133	0.1133	0.2642	0.088	0.088	0.088	0.088
D4	0.1022	0.2161	0.1806	0.2161	0.1762	0.1762	0.1762	0.1762	0.1133	0.1422	0.1422	0.1422	0.1422
D5	0.1022	0.2642	0.1806	0.2642	0.2161	0.2161	0.2161	0.2161	0.2161	0.1133	0.1762	0.1762	0.1762
D6	0.1761	0.1422	0.097	0.1422	0.2642	0.2642	0.2642	0.2642	0.088	0.2642	0.2642	0.2642	0.2642

According to the property diversities of the thirteen decision criteria, they can be divided into three levels. The first level considers safety and environmental friendly properties which contains C1~C4. The second level concerns with thermodynamic qualities including C5~C7. As for the third level, it is made up of C8~C13 with concentrating on techno-economic characteristics. Differential from the semantic score assignment and weighting calculation of criteria in pair-wise matrix established for schemes as shown in Table 7, Table 10 summarizes the pair-wise matrix built for the three levels in GR-I and GR-II, in which the criteria are compared within the same hierarchy. E.g., ranking the relative importance among criteria in the first level, that is C3, C4, C2, and C1. Namely, when comparing C1 with C2, the result is 0 because of C1 is less significant than C2. After the consistency checking of C1~C4 in the first level and arranging the sum of each criterion in descending order, in which the ranking is identical to the importance sequence. Moreover, it is because that the ranking is based on an interval of 1.0, thus, C3 ranks first for getting 3.5 and assigned the semantic score of 1. C4 ranks second and scored 0.919 due to a sum of 2.5. For the criteria in levels two and three, the relative importance rankings are C7, C6, C5 and C11, C13, C12, C10, C8, C9 respectively. Similarly, the semantic score assignment and weighting calculation are performed the same as the first level demonstrated earlier.

Table 10 Consistence checking, semantic score assignment and weighting calculation of decision criteria for three levels

	C1	C2	C3	C4	C5	C6	C7	C8	C9	C10	C11	C12	C13	Sum	Score	Weighting
C1	0.5	0	0	0										0.5	0.739	0.2135
C2	1	0.5	0	0										1.5	0.818	0.2363
C3	1	1	0.5	1										3.5	1	0.2888
C4	1	1	0	0.5										2.5	0.905	0.2614
C5					0.5	0	0							0.5	0.818	0.3004
C6					1	0.5	0							1.5	0.905	0.3324
C7					1	1	0.5							2.5	1	0.3672
C8								0.5	1	0	0	0	0	1.5	0.667	0.141
C9								0	0.5	0	0	0	0	0.5	0.6	0.1269
C10								1	1	0.5	0	0	0	2.5	0.739	0.1563
C11								1	1	1	0.5	1	1	5.5	1	0.2114
C12								1	1	1	0	0.5	0	3.5	0.818	0.173
C13								1	1	1	0	1	0.5	4.5	0.905	0.1914

599 Referring to the last step of three-level fuzzy decision method, the final
600 evaluation results can be acquired by multiplying the weighting matrix of criteria for
601 three levels ($\boldsymbol{W}_i$) and the weighting matrix for schemes ($\boldsymbol{R}_i$). What accounts more is
602 that the first level result should be inserted as last row in $\boldsymbol{R}_i$ of the second level.
603 Furthermore, $\boldsymbol{W}_i$ for second level is multiplying 3/4 as well. And then the
604 equivalent weight needs to be assigned as 1/4 and added in the fourth position of
605 $\boldsymbol{W}_i$ in order to keep the weighting matrix dimension consistency. Repeatedly, the
606 result for the third level can be obtained by substituting 3/4 and1/4 with 6/7 and 1/7.

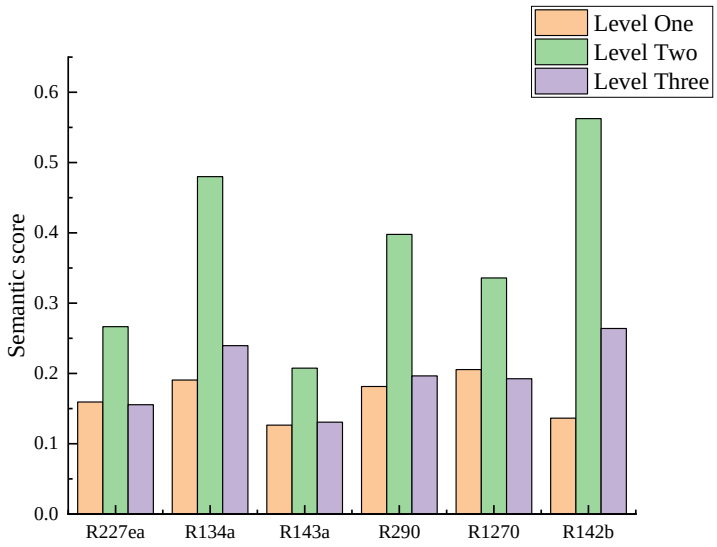

Fig. 9. Results of three-level fuzzy evaluation for GR-I

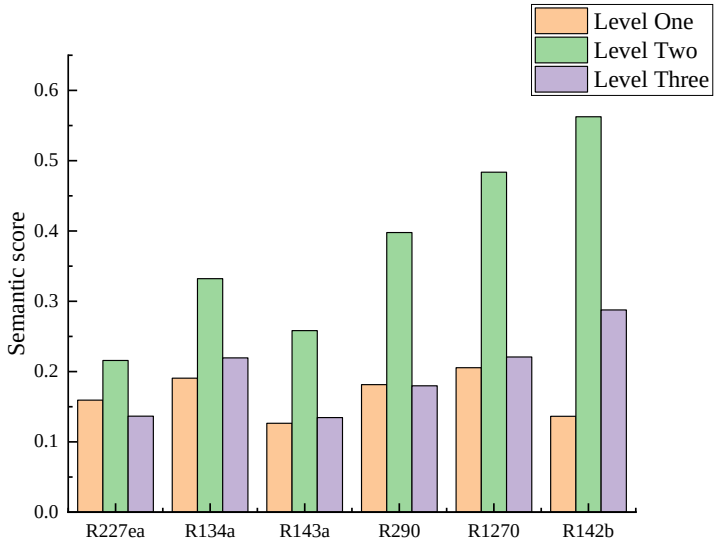

Fig. 10. Results of three-level fuzzy evaluation for GR-II

Figs. 9 and 10 exhibit the comparisons of the three-level evaluation results for GR-I and GR-II. It is concluded that the first level evaluation result are equally in the two geothermal reservoirs. R1270 possess the best reliability when only concerns about safety and environmental friendly properties. The second and third level evaluation results show that R142b is the optimal one which behaves excellent thermodynamic and techno-economic performance among selected working fluids. To the opposite, R143a is not much appropriate for the geothermal operation process according to the three-level evaluation results.

What's more, it is noteworthy that the third level evaluation result for GR-I in Fig.9 is consistent with the optimal ranking result of P_{net} in Table 5. However, comparing the result in Fig.10 and Table 6, which exerts difference between the evaluation and optimal raking order with respect to GR-II. It is implied that the impact of techno-economic indexes on the overall system performance is more apparent at high temperatures.

4 Conclusions

Based on the constructed environmental, thermodynamic and techno-economic assessment models, this paper develops a three-level fuzzy decision method for TORC system used in medium and high temperature geothermal reservoirs. The optimal results of the geothermal TORC system are obtained when P_{net} reaches the maximum. The evaluation results are gained by semantic score assignment, weighting calculation and order ranking. Both of results contribute to the following conclusions:

1. According to the first level evaluation result, the ranking of the working fluid is R1270, R134a, R290, R227ea, R142b and R143a which is identical to both GR-I and GR-II.

2. The second level takes into account the first level result and thermodynamic characteristics, ranking like R142b, R134a, R290, R1270, R227ea, R143a for GR-I and R142b, R1270, R290, R134a, R143a, R227ea for GR-II. It is concluded that R142b is both the most suitable working fluid for its maximal net output power. By contrast of the second level evaluation results for R134a in the two geothermal reservoirs, the heat source with lower temperature and pressure in GR-I is more compatible with it.

3. In terms of the third level, it takes the former two levels results and techno-economic properties into consideration. The evaluation ranking is R142b, R134a, R290, R1270, R227ea and R143a for GR-I. For GR-II ranks R142b, R1270, R134a, R290, R227ea and R143a. From the comprehensive standpoint of the three-level evaluation results, R142b is recommended as best one for the geothermal TORC systems.

The three-level fuzzy decision method developed in this work can effectively figure out the influence of a former level decision criteria on the latter one. The designers can decide on strategies and solutions according to practical requirements by adjusting weighting on indexes. It also helps the investors make whole-scale judgements in the pre-design stage of geothermal ORC system. As for the future work employed with this methodology, it can be extended to analyze the optimization process and make reliable design decisions for different ORC layout.

Acknowledgements

This research work is funded by EPSRC (EP/P028829/1) in United Kingdom.

Reference

[1] Anderson A, Rezaie B. Geothermal technology: Trends and potential role in a sustainable future. Appl Energy 2019; 248:18-34. https://doi.org/10.1016/j.apenergy.2019.04.102.

[2] Statistical review of world energy, https://www.bp.com/en/global/corporate/energy-economics/statistical-review-of-world-energy.html; 2020.

[3] Limberger J, Boxem T, Pluymaekers M et al. Geothermal energy in deep aquifers: A global assessment of the resource base for direct heat utilization. Renew Sustain Energy Rev 2018; 82:961-975. https://doi.org/10.1016/j.rser.2017.09.084.

[4] Moloney F, Almatrafi E, Goswami DY. Working fluid parametric analysis for recuperative supercritical organic Rankine cycles for medium geothermal reservoir temperatures. Renew Energy 2020; 147:2874-2881. https://doi.org/10.1016/j.renene.2018.09.003.

[5] Liang Y, Sun Z, Dong M et al. Investigation of a refrigeration system based on combined supercritical CO2 power and transcritical CO2 refrigeration cycles by waste heat recovery of engine. Int J Refrig 2020; 118:470-482. https://doi.org/10.1016/j.ijrefrig.2020.04.031.

[6] Li XY, Shu GQ, Tian H. Integrating off-design performance in designing CO2 power cycle systems for engine waste heat recovery. Energy Conver Manage 2019; 201:112146. https://doi.org/10.1016/j.enconman.2019.112146.

[7] Song J, Gu CW, Ren XD. Parametric design and off-design analysis of organic Rankine cycle (ORC) system. Energy Conver Manage 2016; 112:157-165. https://doi.org/10.1016/j.enconman.2015.12.085.

[8] Wang X, Shu GQ, Tian H et al. Effect factors of part-load performance for various Organic Rankine cycles using in engine waste heat recovery. Energy Conver Manage 2018; 174:504-515. https://doi.org/10.1016/j.enconman.2018.08.024.

[9] Madhawa Hettiarachchi HD, Golubovic M, Worek WM, Ikegami Y. Optimum design criteria for an Organic Rankine cycle using low-temperature geothermal heat sources. Energy 2007; 32:1698-1706. https://doi.org/10.1016/j.energy.2007.01.005.

[10] Astolfi M, Romano MC, Bombarda P, Macchi E. Binary ORC (organic Rankine cycles) power plants for the exploitation of medium–low temperature geothermal sources – Part A: Thermodynamic optimization. Energy 2014; 66:423-434. https://doi.org/10.1016/j.energy.2013.11.056.

[11] Astolfi M, Romano MC, Bombarda P, Macchi E. Binary ORC (Organic Rankine Cycles) power plants for the exploitation of medium–low temperature geothermal sources – Part B: Techno-economic optimization. Energy 2014; 66:435-446. https://doi.org/10.1016/j.energy.2013.11.057.

[12] Vetter C, Wiemer HJ, Kuhn D. Comparison of sub- and supercritical Organic Rankine Cycles for power generation from low-temperature/low-enthalpy geothermal wells, considering specific net power output and efficiency. Appl Therm Eng 2013; 51:871-879. https://doi.org/10.1016/j.applthermaleng.2012.10.042.

[13] Sun J, Liu Q, Duan Y. Effects of evaporator pinch point temperature difference on thermo-economic performance of geothermal organic Rankine cycle systems. Geothermics 2018; 75:249-258. https://doi.org/https://doi.org/10.1016/j.geothermics.2018.06.001.

[14] Meng D, Liu Q, Ji Z. Performance analyses of regenerative organic flash cycles for geothermal power generation. Energy Conver Manage 2020; 224:113396. https://doi.org/https://doi.org/10.1016/j.enconman.2020.113396.

[15] Cakici DM, Erdogan A, Colpan CO. Thermodynamic performance assessment of an integrated geothermal powered supercritical regenerative organic Rankine cycle and parabolic trough solar collectors. Energy 2017; 120:306-319. https://doi.org/10.1016/j.energy.2016.11.083.

[16] Wang XC, Levy EK, Pan CJ et al. Working fluid selection for organic Rankine cycle power generation using hot produced supercritical CO2 from a geothermal reservoir. Appl Therm Eng 2019; 149:1287-1304. https://doi.org/10.1016/j.applthermaleng.2018.12.112.

[17] Heberle F, Schifflechner C, Bruggemann D. Life cycle assessment of Organic Rankine Cycles for geothermal power generation considering low-GWP working fluids. Geothermics 2016; 64:392-400. https://doi.org/10.1016/j.geothermics.2016.06.010.

[18] Jankowski M, Borsukiewicz A, Wisniewski S, Hooman K. Multi-objective analysis of an influence of a geothermal water salinity on optimal operating parameters in low-temperature ORC power plant. Energy 2020; 202. https://doi.org/10.1016/j.energy.2020.117666.

[19] Mohammadzadeh Bina S, Jalilinasrabady S, Fujii H. Thermo-economic evaluation of various bottoming ORCs for geothermal power plant, determination of optimum cycle for Sabalan power plant exhaust. Geothermics 2017; 70:181-191. https://doi.org/10.1016/j.geothermics.2017.06.007.

[20] Wang JS, Diao MZ, Yue KH. Optimization on pinch point temperature difference of ORC system based on AHP-Entropy method. Energy 2017; 141:97-107. https://doi.org/10.1016/j.energy.2017.09.052.

[21] Zhou GY, Wu E, Tu ST. Optimum selection of compact heat exchangers using non-structural fuzzy decision method. Appl Energy 2014; 113:1801-1809. https://doi.org/10.1016/j.apenergy.2013.07.041.

[22] Manente G, Da Lio L, Lazzaretto A. Influence of axial turbine efficiency maps on the performance of subcritical and supercritical Organic Rankine Cycle systems. Energy 2016; 107:761-772. https://doi.org/10.1016/j.energy.2016.04.063.

[23] Martin H. A theoretical approach to predict the performance of chevron-type plate heat exchangers. Chem Eng Process 1996; 35:301-310. https://doi.org/10.1016/0255-2701(95)04129-x.

[24] Wang Z-Z, Zhao Z-N. Analysis of Performance of Steam Condensation Heat Transfer and Pressure Drop in Plate Condensers. Heat Transfer Eng 1993; 14:32-41. https://doi.org/10.1080/01457639308939809.

[25] Pioro IL, Khartabil HF, Duffey RB. Heat transfer to supercritical fluids flowing in channels—empirical correlations (survey). Nucl Eng Des 2004; 230:69-91. https://doi.org/10.1016/j.nucengdes.2003.10.010.

[26] Imran M, Usman M, Park BS, Yang Y. Comparative assessment of Organic Rankine Cycle integration for low temperature geothermal heat source applications. Energy 2016; 102:473-490. https://doi.org/10.1016/j.energy.2016.02.119.

[27] Kuo WS, Lie YM, Hsieh YY, Lin TF. Condensation heat transfer and pressure drop of refrigerant R-410A flow in a vertical plate heat exchanger. Int J Heat Mass Transf 2005; 48:5205-5220. https://doi.org/10.1016/j.ijheatmasstransfer.2005.07.023.

[28] Turton R, Shaeiwitz JA, Bhattacharyya D, Whiting WB. Analysis, synthesis, and design of chemical processes. 5th ed; 2018.

[29] Jenkins S. 2019 Chemical engineering plant cost index annual average, https://www.chemengonline.com/2019-chemical-engineering-plant-cost-index-annual-average/; 2020.

[30] Zhang C, Liu C, Wang S et al. Thermo-economic comparison of subcritical organic Rankine cycle based on different heat exchanger configurations. Energy 2017; 123:728-741. https://doi.org/10.1016/j.energy.2017.01.132.

A non-structural fuzzy decision method developed for organic Rankine cycles used in liquid-dominated geothermal fields of medium/high temperature

Na Zhang[1], Qinggang Wang[1], Zhibin Yu[2], Guopeng Yu[2,*]

1. School of Civil Engineering and Architecture, East China Jiaotong University, Nanchang, China

2. James Watt School of Engineering, University of Glasgow, United Kingdom, G12 8QQ

Corresponding author: Guopeng.Yu@glasgow.ac.uk

Abstract

A reliable decision-making method is of great importance for the designing of a practical and efficient organic Rankine cycle (ORC) system employed to exploit geothermal energy. This paper develops a three-level non-structural fuzzy decision algorithm for the comprehensive evaluation of a geo-fluid driven trans-critical ORC (TORC) system on the basis of a progressive system performance hierarchy, involving environmental characteristics, safety, thermodynamic and techno-economic performance. Two representative geothermal reservoirs with medium (GR-I) and high (GR-II) temperature are investigated to realize and validate the proposed method. Four mathematical models and six working fluids with thirteen indexes are developed to fulfill the performance evaluation and decision-making courses. Parametric analysis results of the decision criteria are conducted including specific net out power (AP_{net}), thermal efficiency (η_t), exergy efficiency (η_e), heat transfer area per net output power (APR) and electricity production cost (EPC), and the different performance of TORC for GR-I and GR-II are fully revealed. As for the GR-I, the result of the three-level fuzzy decision ranking order is R142b, R134a, R290, R1270, R227ea and R143a. In regard to the GR-II, it's R142b, R1270, R134a, R290, R227ea and R143a. Both show that R142b performs best. In the GR-I and GR-II, R142b obtains the maximal AP_{net} of 110.94kW/(kg·s^{-1}) and 198.14kW/(kg·s^{-1}), the maximal η_t of 14.05% and 14.43%, the maximal η_e of 51.42% and 42.90%, the minimal APR of 0.262(m^2/kW) and 0.185(m^2/kW), the minimal EPC of 0.030($/(kW·h)) and 0.022($/(kW·h)).

Summarily, this three-level fuzzy decision evaluation method can provide important guidance and decisive solution by concisely display the pros and cons for each ORC scheme of geothermal resource utilization.

Keywords: Geothermal energy; Trans-critical ORC; Three-level performance evaluation; non-structural fuzzy decision method

Introduction

Dramatic increase in energy consumption attributes to the fast population expansion and economic growth. A large proportion of energy supply for electricity is currently generated by the combustion of organic fuels, which leads to the growing greenhouse effect and air pollution concerns. For the purpose of human society sustainable progress, renewable resource like geothermal is capable of providing the majority of activities energy with power production, heating and cooling applications [1]. However, the cumulative installed geothermal power capacity in the globe is only increasing from 7.92GW at 2001 to 13.93GW at 2019, which is far away from the growth rate of solar and wind [2]. The conflict between the huge reserve and exploitation of geothermal resources lies in the expensive initial investments [3]. Besides that, the geothermal utilization also relies on the public awareness of environment protection as well as the efficiency enhancement of technologies [1].

The organic Rankine cycle (ORC) has been regarded as a preferred rational solution to harvesting energy from all kinds of heat sources such as waste heat and geothermal reservoirs [4]. Studies on ORC-based waste heat system are devoted to optimizing the engine performance. Liang et al. [5] proposed a small-scale waste heat driven cooling system which integrated supercritical CO_2 power cycle and trans-critical CO_2 refrigeration cycle to recover the waste heat from internal combustion engine and provide cooling energy for refrigerated truck. Li et al. [6] presented a novel framework for analyzing the off-design performance of CO_2 trans-critical power cycle and applied in the heavy-duty truck engine. Song et al. [7] conducted a one-dimensional off-design performance analysis of ORC system by optimizing the turbine aerodynamic model. Wang et al. [8] investigated the part-load performance of ORC system based on the engine waste heat recovery with varying evaporation pressure, condensing condition, working fluid and cycle structure, which revealed that the slower the output power decrease, the better the performance.

Normally, the geothermal heat is categorized as high, medium and low temperature with temperature ranges of >220℃, 220-100℃ and 100-70℃, respectively [9]. The thermodynamic as well as the techno-economic indicators are the major criteria for making investment decisions, which show direct relevance with the utilization benefit of geothermal energy. Summarizing from previous work about geothermal ORC system, researchers are committed to simulating the actual operating process for improving the system thermodynamic and economic performance. Astolfi et al. [10, 11] completed thermodynamic and techno-economic assessments of the ORCs (subcritical, trans-critical, saturated, superheated, regenerative and non-regenerative) for medium temperature geothermal brines. Regarding cycle efficiency and electricity cost as objective functions, the optimization results suggested deploying different cycle layouts that needed to consider the suitable working conditions and economic parameters simultaneously. Vetter et al. [12] analyzed the potential relevance between the maximal net output power and working fluid critical temperature with geothermal fluid temperature in the subcritical and trans-critical ORC system. It found out the highest net output power appeared when the ratio of working fluid critical temperature and geothermal fluid temperature was 0.8. Additionally, the geothermal ORC combined with different subsystem is a feasible way to make system thermo-economic performance better. Sun et al. [13] investigated the effect of pinch point temperature difference (PPTD) on the geothermal ORC thermo-economic performance. The optimization results showed that the optimal evaporation temperature and the heat transfer area

per unit power output decreased with increasing PPTD. The levelized cost of electricity and the dynamic payback period reached minimal when PPTD was 7℃. Meng et al. [14] further explored the interaction between the evaporation and flash temperature on recovering heat from medium temperature geothermal brine. Cakici et al. [15] performed the energy and exergy analysis of trans-critical regenerative ORC system combined with parabolic trough solar collectors. The integrated system net output power increased while the electricity and exergy efficiency decreased compared to single system, and R134a yielded outstanding thermodynamic performance with an increment of the geothermal water inlet temperature and collector areas.

Since the ORC system efficiency depends on the refrigerants properties, researchers also have paid much attention on optimal selection of working fluids with thermodynamic laws assessments. Moloney et al. [4] investigated thermodynamic performance of recuperative trans-critical ORC system for a range of medium to high temperature geothermal reservoirs, indicating that R1233zd(E), R600, R601a, R601, R601b performed the best among twenty working fluids when taken plant efficiency as optimization parameters. Wang et al. [16] developed a working fluid selection methodology mainly based on the thermodynamic performance for the subcritical, superheated, and trans-critical ORC system, utilizing supercritical CO_2 as heat extraction medium in the high temperature geothermal reservoir. The working fluid was recommended when the net output power, specific net output power, thermal efficiency and exergy efficiency were simultaneously equal or greater than their median value. Furthermore, some studies adopt evaluation tool which takes account of environmental properties of working fluids. Heberle et al. [17] qualified the potential of low GWP working fluids like R600, R601a, R290, R1233zd, R1234yf as alternatives for fluorinated fluids like R245fa during the life cycle assessment in the binary geothermal power plant. Judging by the exergy and environmental analysis results, the low GWP working fluids had less effect on environment and higher exergy efficiency in comparison to fluorinated fluids, and the two-stage subcritical ORC and trans-critical ORC manifested better than one-stage subcritical ORC system. For the purpose that avoids the occurrence of refrigerant leakage and guarantees the stable working

conditions of geothermal ORC system, it depends on selecting working fluids with environmental friendly, safety, low flammability and excellent thermodynamic and techno-economic characteristics.

Plenty of investigations are discretely concerned about environmental, thermodynamic and economic performance of geothermal ORC system. But they might neglect the internal relationship between the effective factors. Consequently, a few literatures started to search for multi-objective optimization techniques. Jankowski et al. [18] investigated the influence of geothermal brine salinity on the performance in the subcritical ORC power plant. Taking the minimal heat transfer area and maximal exergy efficiency as the multi-objective parameters under Genetic Algorithm, the Pareto point demonstrated that the heat transfer area increased 8% and exergy efficiency decreased 5% with an increment in salinity. Bina et al. [19] constructed multi-criteria fuzzy TOPSIS decision making method for selecting most favorable cycle configuration in geothermal power plant, covering exergy efficiency, thermal efficiency, net output power, production cost, total cost rate the five indicators. From the thermo-economic perspective and interval Shannon's entropy weighting calculation, the ORC system with internal heat exchanger ranked the first. Wang et al. [20] explored the relationship of pinch point temperature difference (PPTD) between evaporator and condenser in the thermo-economic optimization process of subcritical ORC system. Based on the Analytic Hierarchy Process (AHP) method which cared about the energy output, energy output efficiency and economic criteria, it determined the best working fluid for 150℃ hot water was R11 and the optimal ratio of PPTD was from 1.25 to 1.5.

Although numerous studies have discussed the optimization and evaluation process, the objective indicators just covered relatively limited side and couldn't give a thorough analysis of the overall ORC system performance. The non-structural fuzzy decision method is widely used as an efficient approach for comprehensive evaluation, which considers the indexes interrelation and provides intuitive comparison of the assessed schemes. Zhou et al. [21] adopted non-structural fuzzy decision method for pre-design process of compact heat exchangers which united the thermodynamic, economic and mechanical the three levels evaluation indexes. In the light of the third level evaluation result, the first alternative for sulfuric acid solution cooler was plate-fin heat exchanger fabricated by PTFE.

It can be found that most previous investigations about geothermal ORC system incline to take basis of first and second laws analysis with thermodynamics, focusing on these aspects of thermodynamic and techno-economic performance evaluation, system structure and layout, objective optimization and working fluid selection. Regarding the simulated results of highest net output power or lowest initial investment Cost as criterion to determine the best ORC system scheme. However, the assessment process tends to concentrate on one level decision criteria like thermodynamic indicators, which fails to integrate the comprehensive influence of techno-economic and social benefit indicators on the system whole performance. It may lead the pre-designed scheme to an unachievable goal and cause irretrievable loss to the investors.

Thus, this paper aims at developing an efficient and practical decision-making method, i.e. a three-level non-structural fuzzy decision method, based on comprehensive performance evaluation of the ORC employed for typical geothermal reservoirs. During the whole assessment procedures, six working fluids and three levels of performance are investigated, including the safety and environmental property as the first level, thermodynamic performance as the second level and the techno-economic performance as the third level. A non-structural fuzzy decision-making method is then developed based on the three-level assessment to eventually implement practical and reliable decision-making for the geothermally driven ORC systems.

1 System description

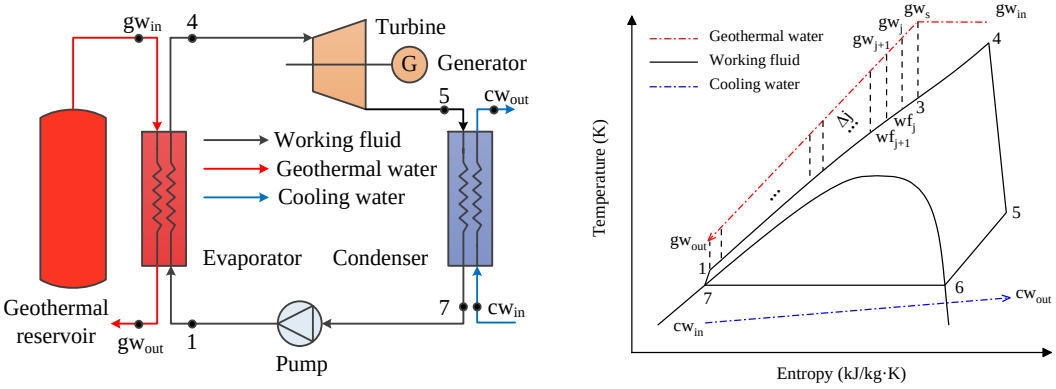

Fig. 1. Schematic and T-s diagram of TORC system

Table 1 Operating conditions of TORC system

Parameter	Value
GR-I wellhead temperature, T_{gwin-1} (℃)	182.23
GR-I wellhead pressure, P_{gw-1} (MPa)	1.06
GR-I wellhead mass flow rate, m_{gw-1} (kg/s)	13.64
GR-II wellhead temperature, T_{gwin-2} (℃)	224.37
GR-II wellhead pressure, P_{gw-2} (MPa)	2.52
GR-II wellhead mass flow rate, m_{gw-2} (kg/s)	11
Condensing temperature, T_{cond} (℃)	35
Cooling water inlet temperature, T_{cwin} (℃)	20
Evaporator pinch point temperature, $T_{pinch-e}$ (℃)	10
Condenser pinch point temperature, $T_{pinch-c}$ (℃)	5
Turbine isentropic efficiency, $\eta_{turbine}$	0.75
Pump isentropic efficiency, η_{pump}	0.7
Dead state temperature, T_{dead} (℃)	20
Dead state pressure, P_{dead} (MPa)	0.101

The geothermal reservoirs under investigation in this work are located in the Aluto Langano geothermal field of Ethiopia, which is recognized as a medium/high temperature liquid-dominated geothermal field in eastern Africa. Two typical and active geothermal reservoirs (i.e., Geothermal Reservoir I and Reservoir II) are chosen as heat source for the proposed system. They produced two-phase, fluid-dominated wellhead discharge, and the discharge data from wellhead tests are gathered and listed in Table 1. Wellhead pressure, temperature and mass flow rate are tested in situ. Instead of choosing the basic sub-critical ORC pattern, the trans-critical ORC (TORC) is determined for its higher energy efficiency, lower exergy loss and modest pressure requirement [22]. The primary TORC system working conditions constructed for working fluids in the GR-I (182.23℃) and GR-II (224.37℃) are nearly identical except the investigated evaporation pressure and turbine inlet temperature and flow channels in heat exchangers. Table 1 lists the detailed value of relevant parameters for TORC design and construction. As demonstrated in the semantic definition of TORC, the working fluid is compressed to exceed critical pressure via pump. And it absorbs heat from geothermal water to vaporize until it reaches the highest temperature during the courses of evaporation. Then, the supercritical working fluid discharges into the turbine to produce output shaft work which can be employed for power generation. After expansion, the subcritical overheated vapor is condensed into saturated liquid by cooling water before flowing into the pump to accomplish the next cycle. The schematic and T-s diagram is illustrated in Fig. 1. The T-s diagram also shows the segment-iterative

process of seeking pinch point temperature between the heat source and working fluids.

Table 2 Fluid characteristics [4, 16]

Working Fluid	Thermodynamic Property						Environmental Property			
	M /(kg·kmol^{-1})	T_b /℃	T_{de} /K	T_{cr} /K	P_{cr} /MPa	Behavior	Safety Level	ALT/Year	ODP	GWP/(100 years)
R227ea	170.0289	-16.341	475	374.9	2.925	dry	A1	38.9	0	3320
R134a	102.032	-26.0738	455	374.21	4.0593	wet	A1	13.4	0	1430
R143a	84.041	-47.2406	650	345.857	3.761	wet	A2L	47.1	0	4470
R290	44.0956	-42.1138	650	369.89	4.2512	wet	A3	0.034	0	5
R1270	42.0797	-47.6192	575	364.211	4.555	wet	A3	0.001	0	1.8
R142b	100.495	-9.1233	470	410.26	4.055	isentropic	A2	17.2	0.065	2310

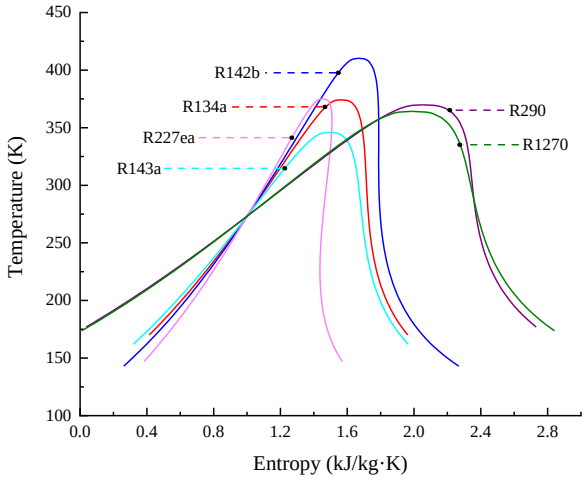

Fig. 2. T-s diagram of selected working fluids

The operating process of TORCs for two geothermal reservoirs are simulated in MATLAB with six picked working fluids, the environmental and thermodynamic characteristics of each working fluid are displayed in Table 2 and Fig. 2. The principals for selecting working fluids are subject to the safety level, atmospheric life time (ALT), ozone depletion potential (ODP) and global warming potential (GWP).

For the safety level, A and B imply the toxicity grades while B is higher than A. Number 1, 2, 2L and 3 indicate flammability level and increase progressively. ALT represents existing time at the atmosphere if leakage of refrigerant happens, ODP means the ozone consumption with refrigerant diffusing into ozone layer, and GWP indicates the potential of temperature increase in the global world caused by inappropriately release of refrigerant. With regard to the four environmental indicators, the smaller value the better performance. And the iteration ranges of turbine inlet temperature are higher than critical temperature but lower than working fluids decomposition temperature. Furthermore, the assumptions stated as below are taken into consideration:

- Each TORC system is operating steadily.
- No impurity like silica exists in the geothermal water, as result its outlet temperature is allowed for lower than 70℃.
- The pressure drop and heat losses are neglected during each part of performing process.
- The ambient temperature and pressure are 20℃ and 101kPa.
- The pinch point temperature in the evaporator and condenser are 10℃ and 5℃ respectively.

2 Mathematical modelling

2.1 Thermodynamic model

Based on the first and second laws of thermodynamics, the following formulas are introduced to calculate thermodynamic assessment indexes.

The heat transfer flow rate in the evaporator:

$$Q_{evaporator} = m_{wf}\left(h_4 - h_1\right) \tag{1}$$

The heat transfer flow rate in the condenser:

$$Q_{condenser} = m_{wf}\left(h_5 - h_7\right) \tag{2}$$

The consumed power of pump:

$$P_{pump} = m_{wf}\left(h_1 - h_7\right) \tag{3}$$

The turbine output shaft power:

$$P_{turbine} = m_{wf}\left(h_4 - h_5\right) \tag{4}$$

The net output power of TORC system:

$$P_{net} = P_{turbine} - P_{pump} \tag{5}$$

The specific net output power:

$$AP_{net} = P_{net} / m_{gw} \tag{6}$$

The thermal efficiency of TORC system:

$$\eta_t = P_{net} / Q_{evaporator} \times 100\% \tag{7}$$

Where m_{wf} and m_{gw} are the mass flow rate of working fluid and geothermal water, while h_i represents the specific state enthalpy with $i = 1...7$ as shown in Fig. 1.

The exergy of each state point:

$$E_i = m\left[\left(h_i - h_0\right) - T_0\left(s_i - s_0\right)\right] \tag{8}$$

Where m is the mass flow rate of objective fluid, while s_i represents the state point entropy with $i = 1...7$, and the subscript 0 implies the ambient condition.

The exergy losses of pump:

$$I_{pump} = m_{wf} T_0\left(s_1 - s_7\right) \tag{9}$$

The exergy losses of evaporator:

$$I_{evaporator} = \left(E_{gwin} + E_1\right) - \left(E_{gwout} + E_4\right) \tag{10}$$

The exergy losses of turbine:

$$I_{turbine} = m_{wf} T_0\left(s_5 - s_4\right) \tag{11}$$

The exergy losses of condenser:

$$I_{condenser} = \left(E_{cwin} + E_5\right) - \left(E_{cwout} + E_7\right) \tag{12}$$

The exergy losses caused by cooling water flows out:

$$I_{out}^{cooling\ water} = E_{cwout} - E_{cwin} \tag{13}$$

The total exergy losses of TORC system:

$$I_{system} = I_{pump} + I_{evaporator} + I_{turbine} + I_{condenser} + I_{out}^{cooling\ water} \tag{14}$$

The net exergy that geothermal water flows into system:

$$E_{in}^{gw} = P_{net} + I_{system} \tag{15}$$

The exergy efficiency of TORC system:

$$\eta_e = P_{net} / E_{in}^{gw} \tag{16}$$

The subscript *in* and *out* refers to the inlet and outlet state for objective fluid.

Before calculating the overall heat transfer coefficient and area of heat exchangers, the primary task is to identify the mass flow rate of working fluid. The inlet temperature (T_{gwin}) and mass flow rate of geothermal water (m_{gw}) are constant. Besides that, the minimal temperature difference is set larger than 10℃ between the evaporator inlet temperature of geothermal water and outlet temperature of working fluid.

First of all, referring to the Pinch Point Temperature Difference method, the evaporator outlet temperature of geothermal water (T_{gwout}) is assumed to get the outlet enthalpy (h_{gwout}) and calculate initial value of working fluid mass flow rate (m_{wf}):

$$m_{wf} = m_{gw}\left(h_{gwin} - h_{gwout}\right)\Big/\left(h_4 - h_1\right) \tag{17}$$

Secondly, the singe-phase flow region of geothermal water from gw_s to gw_{out} point is divided into one hundred segments as shown in Fig. 1. Thus the temperature difference of each segment can be determined. As a result, it could deduce the next state point temperature (T_{gwj}) from the beginning of T_{gws}.

$$T_{gwj} = T_{gws} - \left(T_{gws} - T_{gwout}\right)\Big/100\,j \tag{18}$$

The subscript j denotes the divided segments which range from 1 to 100.

Thirdly, based on the acquired variables of h_{gwj}, h_{gwout}, m_{wf}, the enthalpy (h_{gwj}) and temperature (T_{gwj}) of each state point for working fluids from 1 to 3 point can be obtained by using the first laws of thermodynamics.

$$h_{wfj} = h_1 + m_{gw}\left(h_{gwj} - h_{gwout}\right)\Big/m_{wf} \tag{19}$$

Lastly, the actual temperature difference between geothermal water and working fluids of each segment can be calculated. And the minimal temperature difference (ΔT_{act}) could be found out. Comparing it with 10℃, if the discrepancy satisfies the accuracy requirement (1%), it demonstrates that the assumed evaporator outlet temperature of geothermal water is reasonable. Otherwise, it needs to go back to the first step to presume another outlet temperature until meets the accuracy requirement.

2.2 Heat transfer model

The plate heat exchanger is selected as evaporator and condenser for its excellent heat transfer performance and compact structure. The geometric structure and dimension of plate heat exchanger are summarized in Table 3.

Table 3 Geometry of plate heat exchanger

Parameter	Value
Chevron angle, β (°)	60
Plate width, L_w (m)	0.65
Plate thickness, t (m)	0.0005
Corrugation pitch, Λ (m)	0.0085
Corrugation depth, b (m)	0.0025
Surface enlargement factor, ϕ	1.19
Hydraulic diameter, D_h (m)	0.0042
Equivalent diameter, D_{eq} (m)	0.005
Coefficient of thermal conductivity, λ_{PHE} (kW/(m·K))	0.0163

The heat transfer process in the evaporation and condenser are both divided into two sections. As illustrated above, the evaporator separates into single-phase flow and two-phase flow region according to the thermo-physical state of geothermal water. Similarly, the heat transfer area of condenser is divided into cooling and condensing region on the basis of the thermo-physical state of working fluid.

For the single-phase flow of geothermal water in the evaporator and cooling water in the condenser, the Leveque correlation [23] is used to calculate the heat transfer coefficient, which are α_{sgw} and α_{cw} respectively.

The Wang and Zhao correlation [24] is applied for calculation of geothermal water two-phase flow heat transfer coefficient (α_{tgw}) in the evaporator.

$$Nu = 0.00115\left(\mathrm{Re}_l / H\right)^{0.983} \mathrm{Pr}_l^{0.33} \left(\rho_l / \rho_v\right)^{0.248} \tag{20}$$

$$\alpha_{tgw} = Nu\lambda_l / D_{eq} \tag{21}$$

$$\mathrm{Re}_l = G_{gw}\left(1 - x_0\right) D_{eq} / \mu_l \tag{22}$$

$$\mathrm{Pr}_l = c_{p,l}\mu_l / \lambda_l \tag{23}$$

$$H = c_{p,l}\left(T_{ave} - T_{wall}\right) \Big/ \left(i_{fg} + 0.68 c_{p,l}\left(T_{ave} - T_{wall}\right)\right) \tag{24}$$

Where the indicators with subscript l are calculated based on the mean temperature of steam and wall temperature (T_{ave}), and the indicators with subscript v are calculated based on the average steam temperature, λ represents the thermal conductivity of objective water, G_{gw} implies the total mass flux of geothermal water, x_0 is the vapor quality at the end state of two-phase flow region which sets as 0, D_{eq} is the equivalent diameter of plate heat exchanger, and i_{fg} represents the latent heat of water from liquid to vapor state.

As for the tans-critical working fluids in evaporator, Jackson correlation [25] is adopted to calculate the heat transfer coefficient ($\alpha_{tc,wf}$).

$$Nu = 0.0183\,\mathrm{Re}^{0.82}\,\mathrm{Pr}^{0.5}\left(\rho_{wall}/\rho\right)^{0.3}\left(\overline{c_p}/c_p\right)^{n} \tag{25}$$

$$\alpha_{tc,wf} = Nu\lambda/D_h \tag{26}$$

$$\overline{c_p} = \left(h_{wall} - h_c\right)/\left(T_{wall} - T_c\right) \tag{27}$$

$$\mathrm{Re} = \rho v D_h/\mu \tag{28}$$

$$\mathrm{Pr} = c_p\mu/\lambda \tag{29}$$

$$\begin{aligned} &n = 0.4,\ T_c < T_{wall} < T_{cri},\ 1.2T_{cri} < T_c < T_{wall} \\ &n = 0.4 + 0.2\left[\left(T_{wall}/T_{cri}\right) - 1\right],\ T_c < T_{cri} < T_{wall} \\ &n = 0.4 + 0.2\left[\left(T_{wall}/T_{cri}\right) - 1\right]\left[1 - 5\left(T_c/T_{cri} - 1\right)\right],\ T_{cri} < T_c < 1.2T_{cri},\ T_c < T_{wall} \end{aligned} \tag{30}$$

Where T_c is the characteristic temperature of working fluid and h_c is obtained based on it. Additionally, other indexes like ρ_{wall} and h_{wall} are acquired under the condition of plate heat exchanger wall-side temperature (T_{wall}), T_{cri} is the critical temperature of working fluid, and D_h is hydraulic diameter which calculated by $D_h = 2b/\phi$.

For the cooling part in the condenser, the Chisholm correlation [26] is employed for calculating the working fluid heat transfer coefficient (α_{swf}).

For the condensing part in the condenser, the Kandlikar correlation [27] is used to calculate the working fluid heat transfer coefficient (α_{twf}).

$$\alpha_l = 0.2092\left(\lambda_l / D_h\right)\mathrm{Re}_l^{0.78}\,\mathrm{Pr}_l^{0.33}\left(\mu/\mu_{wall}\right)^{0.14} \tag{31}$$

$$\mathrm{Re}_l = G_{wf}\,D_h/\mu_l \tag{32}$$

$$\mathrm{Pr}_l = c_{p,l}\,\mu_l/\lambda_l \tag{33}$$

$$Co = \left(\rho_v/\rho_l\right)\left(1/x_m - 1\right)^{0.8} \tag{34}$$

$$Fr_l = G_{wf}^2 \Big/ \left(\rho_l^2 g D_h\right) \tag{35}$$

$$Bo = q/G_{wf} i_{fg} \tag{36}$$

$$\alpha_{twf} = \alpha_l\left(0.25Co^{-0.45}Fr_l^{0.25} + 75Bo^{0.75}\right) \tag{37}$$

Where g implies the acceleration of gravity which is 9.8(m/s^2), G_{wf} is the total mass flow rate of working fluid, and x_m is the vapor quality which sets 0.5.

After acknowledging the heat transfer coefficient of each section, the heat exchanger areas (A) are derived from the following equations.

$$A = Q/U/\Delta T_m \tag{38}$$

$$1/U = 1/\alpha_{hot-side} + t/\lambda_{PHE} + 1/\alpha_{cold-side} \tag{39}$$

Where Q is the heat transfer mass flow and U is the overall heat transfer coefficient of each part, while ΔT_m is the log mean temperature difference between hot-side and cold-side and λ_{PHE} is the thermal conductivity of plate heat exchanger.

2.3 Techno-economic model

For the purpose of giving an all-around viewpoint on the techno-economic properties of the ORC system, six parameters are collected that covered two aspects of investment and expected return. In detail, which are heat transfer area per net output power (APR), turbine characteristic size parameters (SP), gross cost based on the latest economic indexes ($\mathrm{Cos}t_{2019}$), electricity production cost (EPC), depreciated payback period (DPP) and saving to investment ratio (SIR).

The APR is employed as evaluation criterion of the heat exchanger compactness, the more compact of the heat exchanger structure, the smaller the APR and the lower the initial investment, which is defined as:

$$APR = \left(A_e + A_c\right) / P_{net} \tag{40}$$

The SP is regarded as an indicator of the relative cost of TORC system by measuring the size of turbine, which is defined as:

$$SP = \sqrt{V_5} / \Delta h_{isen}^{0.25} \tag{41}$$

Where V_5 is the volume flow of turbine outlet (state point 5) while Δh_{isen} is isentropic enthalpy drop before and after expansion (state point 4 to 5).

The $\mathrm{Cos}t_{2019}$ is determined based on the Module Cost Technique [28], It represents the sum of bare module costs of the main components in ORC system, which is given below:

$$\mathrm{Cos}t_{2001} = \mathrm{C}_{BM,\,pump} + \mathrm{C}_{BM,\,evaporator} + \mathrm{C}_{BM,\,turbine} + \mathrm{C}_{BM,\,condenser} \tag{42}$$

$$\mathrm{Cos}t_{2019} = \mathrm{Cos}t_{2001} CEPCI_{2019} / CEPCI_{2001} \tag{43}$$

Where $CEPCI$ is the chemical engineering plant cost index while $CEPCI_{2001} = 397$ and $CEPCI_{2019} = 607.5$ [29].

As presented in Table 4, the bare module cost (C_{BM}) is defined as the product of purchased cost (C_p) and bare module cost factor (F_{BM}). C_p is related to the capacities ($P_{pump}, P_{turbine}$) and size parameters (A_e, A_c) of each component which are acquired from the optimal results. F_{BM} considers the material factor (F_M) and pressure factor (F_P). The materials for heat exchangers and pump are stainless steel and the pump type is centrifugal. Then, the coefficients like B, C, K could be determined by the arranged configurations.

Table 4 Main components bare module cost equations

Component	Bare module cost equation	Coefficient				
		$K_1/K_2/K_3$	$C_1/C_2/C_3$	B_1/B_2	F_M	F_{BM}
Turbine	$C_{BM,turbine} = C_{p,turbine} F_{BM,turbine}$ $\lg C_{p,turbine} = K_{1,t} + K_{2,t} \lg P_t + K_{3,t} (\lg P_t)^2$	$K_{1,t} = 2.626$ $K_{2,t} = 1.440$ $K_{3,t} = -0.178$	/	/	/	3.5
Pump	$C_{BM,pump} = C_{p,pump} F_{BM,pump}$ $\lg C_{p,pump} = K_{1,p} + K_{2,p} \lg P_p + K_{3,p} (\lg P_p)^2$ $F_{BM,pump} = B_{1,p} + B_{2,p} F_{M,pump} F_{P,pump}$ $\lg F_{p,pump} = C_{1,p} + C_{2,p} \lg P_P + C_{3,p} (\lg P_p)^2$	$K_{1,p} = 3.389$ $K_{2,p} = 0.054$ $K_{3,p} = 0.155$	$C_{1,p} = -0.394$ $C_{2,p} = 0.396$ $C_{3,p} = -0.002$	$B_{1,p} = 1.89$ $B_{2,p} = 1.35$	2.32	/
Evaporator	$C_{BM,evaporator} = C_{p,evapoeator} F_{BM,evaporator}$ $\lg C_{p,evaporator} = K_{1,e} + K_{2,e} \lg A_e + K_{3,e} (\lg A_e)^2$ $F_{BM,evaporator} = B_{1,e} + B_{2,e} F_{M,evaporator}$	$K_{1,e} = 4.666$ $K_{2,e} = -0.156$ $K_{3,e} = 0.155$	/	$B_{1,e} = 0.96$ $B_{2,e} = 1.21$	2.45	/
Condenser	$C_{BM,condenser} = C_{p,condenser} F_{BM,condenser}$ $\lg C_{p,condenser} = K_{1,c} + K_{2,c} \lg A_c + K_{3,c} (\lg A_c)^2$ $F_{BM,condenser} = B_{1,c} + B_{2,c} F_{M,condenser}$	$K_{1,c} = 4.666$ $K_{2,c} = -0.156$ $K_{3,c} = 0.155$	/	$B_{1,c} = 0.96$ $B_{2,c} = 1.21$	2.45	/

The EPC demonstrates the relative scales of capital input and output from the perspectives of per unit power generation cost, which is presented as:

$$EPC = \left(\mathrm{Cost}_{2019} CRF + f_k \,\mathrm{Cost}_{2019}\right) \Big/ \left(P_{net} h_{working-time}\right) \tag{44}$$

$$CRF = i(1+i)^{time} \Big/ \left((1+i)^{time} - 1\right) \tag{45}$$

Where CRF is the capital recovery factor, f_k is operation and maintenance factor which sets as 1.65%, $h_{working-time}$ is the working time of each year which assumes to be 8100h, i is the annual interest which regarded as 5% and $time$ is the life cycle assessment time of 15 years.

The DPP gives a clearly projected investment return time of the ORC system, which is defined as:

$$DPP = -\ln\left(1 - k\,\mathrm{Cost}_{2019} / F_{n0}\right) \big/ \ln(1+k) \tag{46}$$

$$F_{n0} = E_P \left(P_{net} h_{working-time}\right) - f_k \,\mathrm{Cost}_{2019} \tag{47}$$

Where k implies the depreciated ratio which is 5%, F_{n0} is the system net income and E_P is the electricity sale price which sets as 0.1($/kW·h) [30]. Moreover, the net output power (P_{net}) is completely regarded as net electricity generation as result that the power generation efficiency sets as 1.

The SIR figures out the proportion of the predicted profit and initial investment, which is defined as:

$$SIR = B_{time} / C_{time} \tag{48}$$

$$B_{time} = \sum_{j=1}^{time} \left(P_{net} h_{working-time} E_p (1+r)^j \Big/ (1+i)^j\right) \tag{49}$$

$$C_{time} = \sum_{j=0}^{time} \left(\left(f_k \,\mathrm{Cost}_{2019}\right)(1+r)^j \Big/ (1+i)^j\right) \tag{50}$$

Where B_{time} and C_{time} are the net value of total income and investment during the period of life cycle assessment time which $j=1...15$, r is the inflation rate which sets as 2.9%.

2.4 Three-level fuzzy decision model

In the paper, the three-level fuzzy decision model is established based on the properties model of working fluids, the thermodynamic model and the techno-economic model as put forward earlier, which are regarded as the first, second and third level respectively. The development and programming of the method is accomplished by the following four steps:

Step (1) - Acquiring the optimal results of decision criteria by choosing appropriate indicator as the objective function according to the realistic operation requirements.

Step (2) - A pair-wise comparison matrix of each decision criterion for schemes is constructed so as to rank in sequence and assign the semantic score. After the normalization of semantic score, the weighting set of each criterion could be obtained.

Step (3) - Similar to step two, a pair-wise comparison matrix of each decision criterion for three classified levels is built, the weighting set calculation is subject to the relative importance of decision criteria within each level.

Step (4) - After acknowledging the weighting set of each criterion, the weighting matrix for schemes ($\boldsymbol{R}_i$) and levels ($\boldsymbol{W}_i$) can be developed. And the evaluation set ($\boldsymbol{B}_i$) can be calculated by the following equation:

$$\boldsymbol{B}_i = \boldsymbol{W}_i \times \boldsymbol{R}_i \tag{51}$$

For the second level, evaluation result of the first level should be inserted into the $\boldsymbol{R}_i$ as the last row. The original $\boldsymbol{W}_i$ of second level needs to multiply $n/(n+1)$ if n decision criteria are included. Next, a new $\boldsymbol{W}_i$ has to be formed by assigning $1/(n+1)$ in the final position of the former one. For the third level, the same procedure is undergoing repeatedly to gain $\boldsymbol{B}_i$.

Summarizing the three mathematical models above, Fig. 3 gives a clear flow chart of the construction procedures.

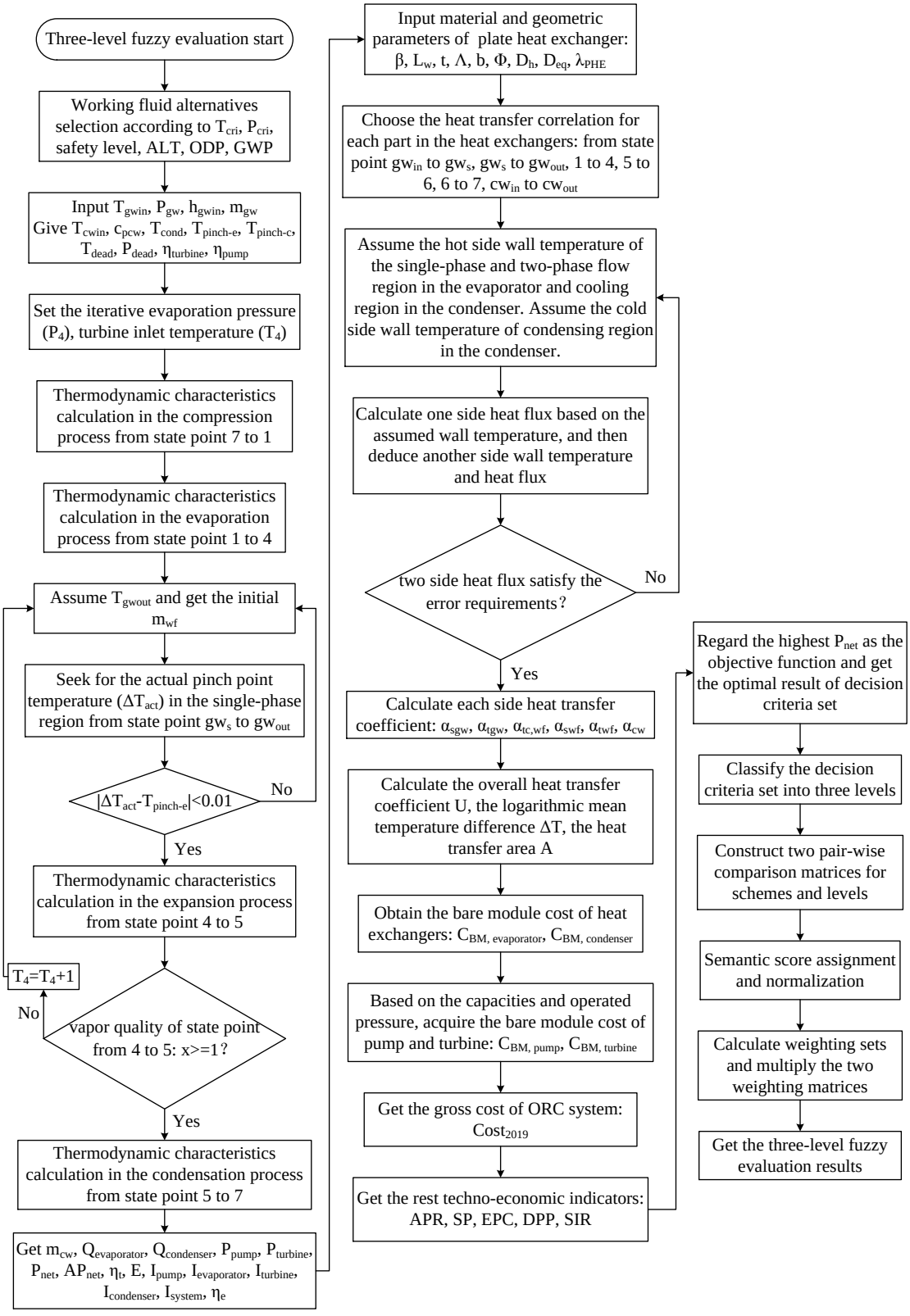

Fig. 3. The three-level fuzzy evaluation procedures

3 Results and discussion

3.1 Thermodynamic performance

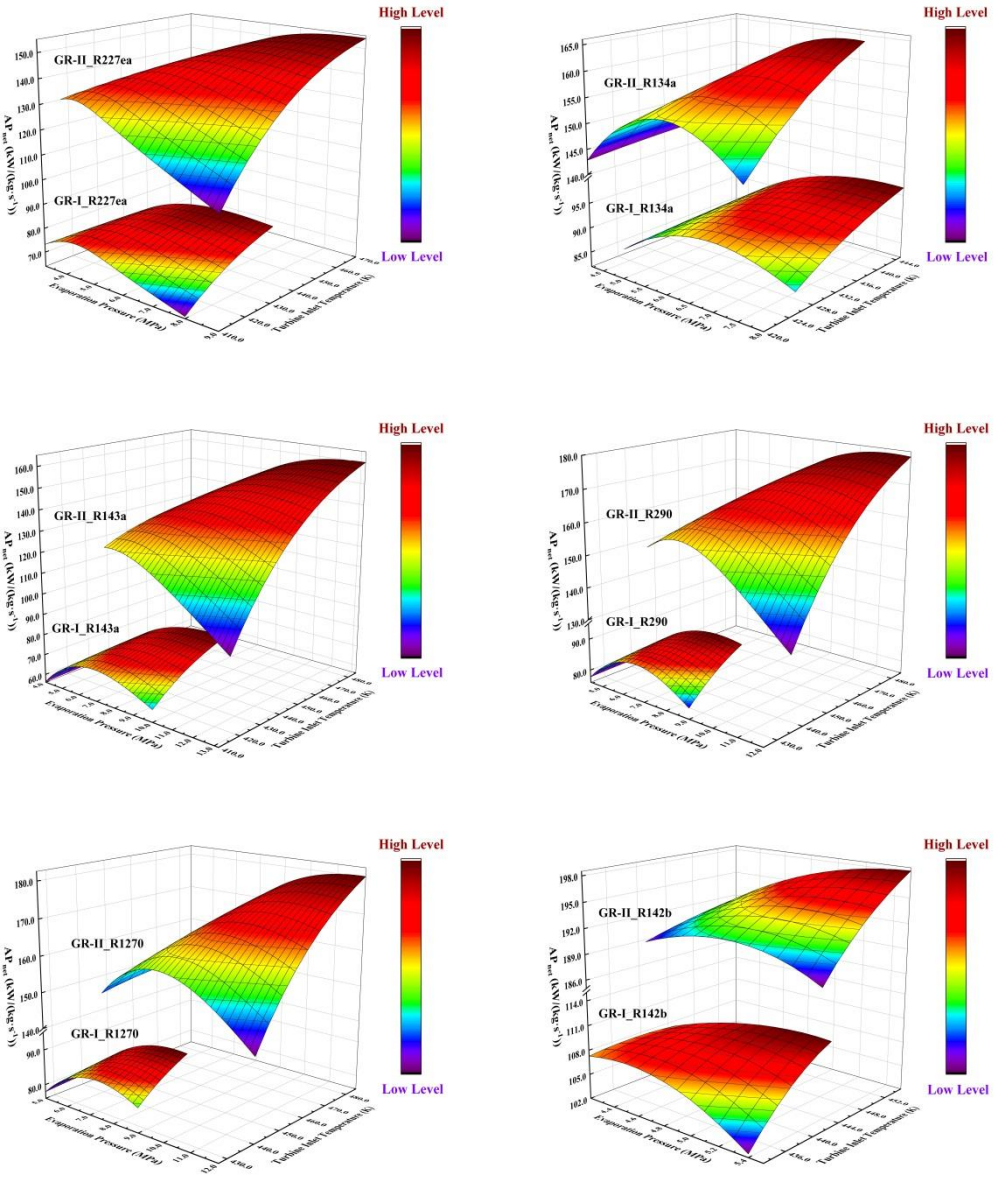

Fig. 4. Specific net output power (AP_{net}) variation in two geothermal reservoirs

In this study, the specific net output power (AP_{net}), thermal efficiency (η_t) and exergy efficiency (η_e) are determined to estimate the thermodynamic performance of the TORC system designed for both geothermal reservoirs (GR-I and GR-II). As shown in Figs. 4, 5 and 6, the overall variation of the three indexes shows both similarities and diversities with increasing evaporation pressure (P_4) and turbine inlet temperature (T_4) for each working fluid in two different geothermal reservoirs. Moreover, Fig. 4 indicates AP_{net} of the six selected working fluids in GR-II which ranges from 93.73-198.14kW/(kg·s^{-1}) is apparently higher than that of GR-I which is from 56.46-110.94kW/(kg·s^{-1}), indicting a higher power capacity of GR-II. Besides, Fig. 4 demonstrates AP_{net} increases firstly and then decreases when raising P_4 under given T_4. It is because turbine output shaft power ($P_{turbine}$) enhances obviously while P_4 increases from lower values (but still exceed the critical pressure of the working fluid). And the consumed power of pump (P_{pump}) increases more rapidly than $P_{turbine}$ with further increase of P_4, which results that the upward trend of AP_{net} gradually slows down until it starts deceasing. In addition, due to the limits of pinch point temperature difference ($T_{pinch-e}$) and decomposition temperature (T_{de}) of working fluids, AP_{net} keeps increasing while T_4 grows up to reach the maximal value under higher P_4. Furthermore, AP_{net} shows upward tendency firstly and then goes downward when given a lower P_4. Comparing the optimal results of working fluids in GR-I, R142b is able to acquire the largest AP_{net} of 110.94kW/(kg·s^{-1}) at the condition that the P_4 is 5.2MPa and T_4 is 445K. On the contrary, R143a obtains smallest AP_{net} of 81.77kW/(kg·s^{-1}) in the case of the

460 P_4 is 9.4MPa and T_4 is 445K. With regard to GR-II, R142b maintains the highest

461 AP_{net} as well, which is 198.14kW/(kg·s^{-1}) when the P_4 is 5.5MPa and T_4 is

462 455K. And R227ea yields lowest AP_{net} of 154.02kW/(kg·s^{-1}), for the P_4 is

463 8.6MPa and T_4 is 470K.

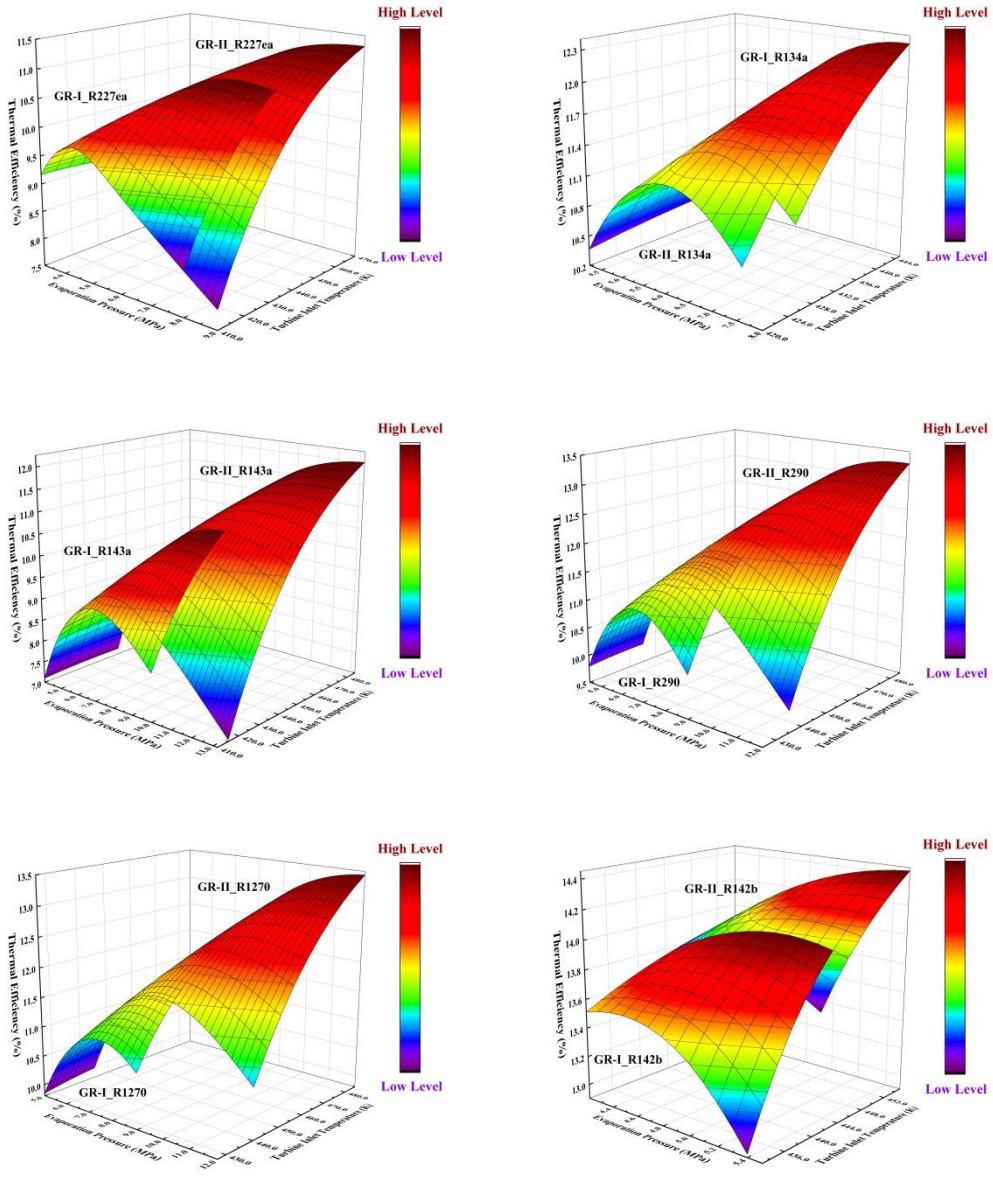

Fig. 5. Thermal efficiency (η_t) variation in two geothermal reservoirs

Thermal efficiency (η_t) is defined as the ratio of net power output (P_{net}) to the amount of heat absorbed during the evaporation process, as shown in Eq. (7). The change of η_t by varying evaporation pressure (P_4) and turbine inlet temperature (T_4) is illustrated in Fig. 5. As far as the η_t of each working fluid is concerned, there exists regions that are partially overlapped between GR-I and GR-II, which ranges from 7.10-14.05% and 7.04-14.43%, indicating that even though geothermal reservoirs have different power capacities, they could have similar energy conversion efficiency ranges applying TORC. Specifically, it is observed that η_t of all selected working fluids can be described as increasing and dropping later with an increase of P_4 under investigated T_4. The alteration of η_t is similar with AP_{net}. For this reason, the η_t rises faster at lower P_4 and stabilizes till it decreases as P_4 increases further. Additionally, with the restrictions of $T_{pinch-e}$ and T_{de}, η_t represents an inclination of rising up continuously with increasing T_4 to the maximum under higher P_4. The reason can be explained from that, although the enthalpy difference ($h_4 - h_5$) becomes larger and the mass flow rate of working fluids (m_{wf}) is declining in the course of expansion, the turbine output shaft power ($P_{turbine}$) still increases and the pump power consumption (P_{pump}) decreases as T_4 continues increasing. In the meanwhile, when the system operates at a lower P_4, η_t behaves in a trend of increasing first and then diminishes as T_4 grows up. The maximum results of η_t for working fluids in GR-I and GR-II are both R142b which are 14.05% and 14.43% respectively, for the P_4 and T_4 are 5.1MPa, 445K and 5.5MPa, 455K. To the opposite, R143a and R227ea have the minimal η_t in GR-I and GR-II with

the values of 10.66% and 11.32%.

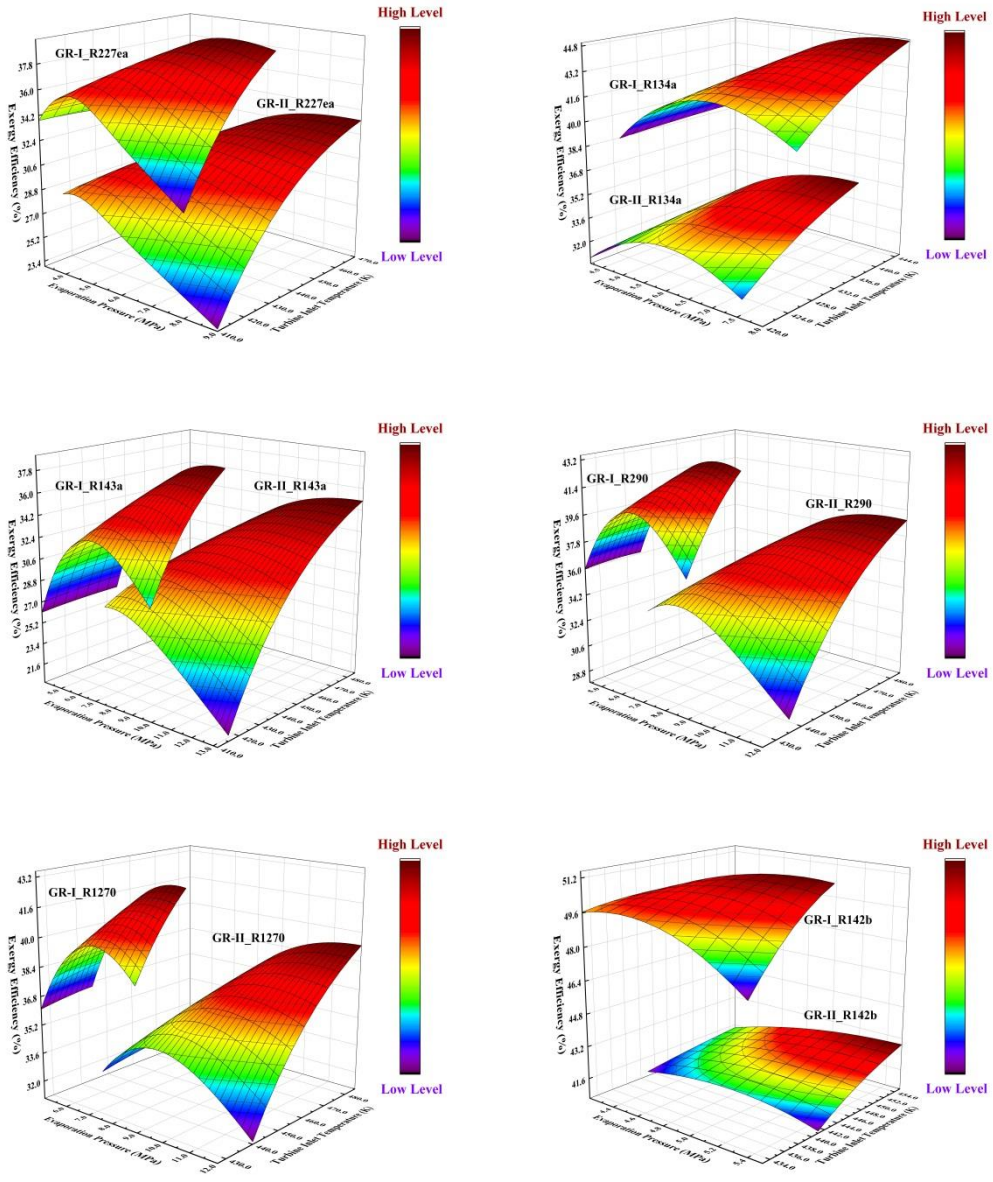

Fig. 6. Exergy efficiency (η_e) variation in two geothermal reservoirs

Exergy signifies the greatest beneficial output power that geothermal system possesses. The exergy efficiency (η_e) is employed for assessing the exergy utilization, which is characterized as the ratio of net output power (P_{net}) to the net exergy flows into the system (E_{in}^{gw}), as given in Eq. (16). Typically, it can be noticed from Fig. 6 that the η_e in GR-I is normally higher than GR-II. The ranges are 26.11-51.42% for GR-I and 23.14-42.89% for GR-II, which indicates that although GR-I has smaller power capacity, the exergy is fully utilized compared to GR-II. Particularly, Fig. 6 denotes that the arc-surface changing trend of η_e is familiar with that of AP_{net} and η_t. Increasing of η_e is owing to the thermal matching performance becomes better between heat sources and working fluids and the exergy loss (I_{system}) reduces constantly with an increment of lower evaporation pressure (P_4). Instead, the reduction of P_{net} is more markedly than the I_{system} decreases with further increase of P_4, leading to the downward tendency for η_e. What's more, the η_e shows a trend of growing up for that P_{net} keeps increasing while I_{system} turns into dropping by improving turbine inlet temperature (T_4) under investigated P_4. According to optimal results of the working fluids, R142b achieves the biggest η_e of 51.42% and 42.90% in the GR-I and GR-II, with the P_4 and T_4 are 5.2MPa, 445K and 5.5MPa, 455K. And R143a and R227ea get lowest exergy efficiency of 38.30% and 33.42% for the two geothermal reservoirs.

3.2 Techno-economic performance

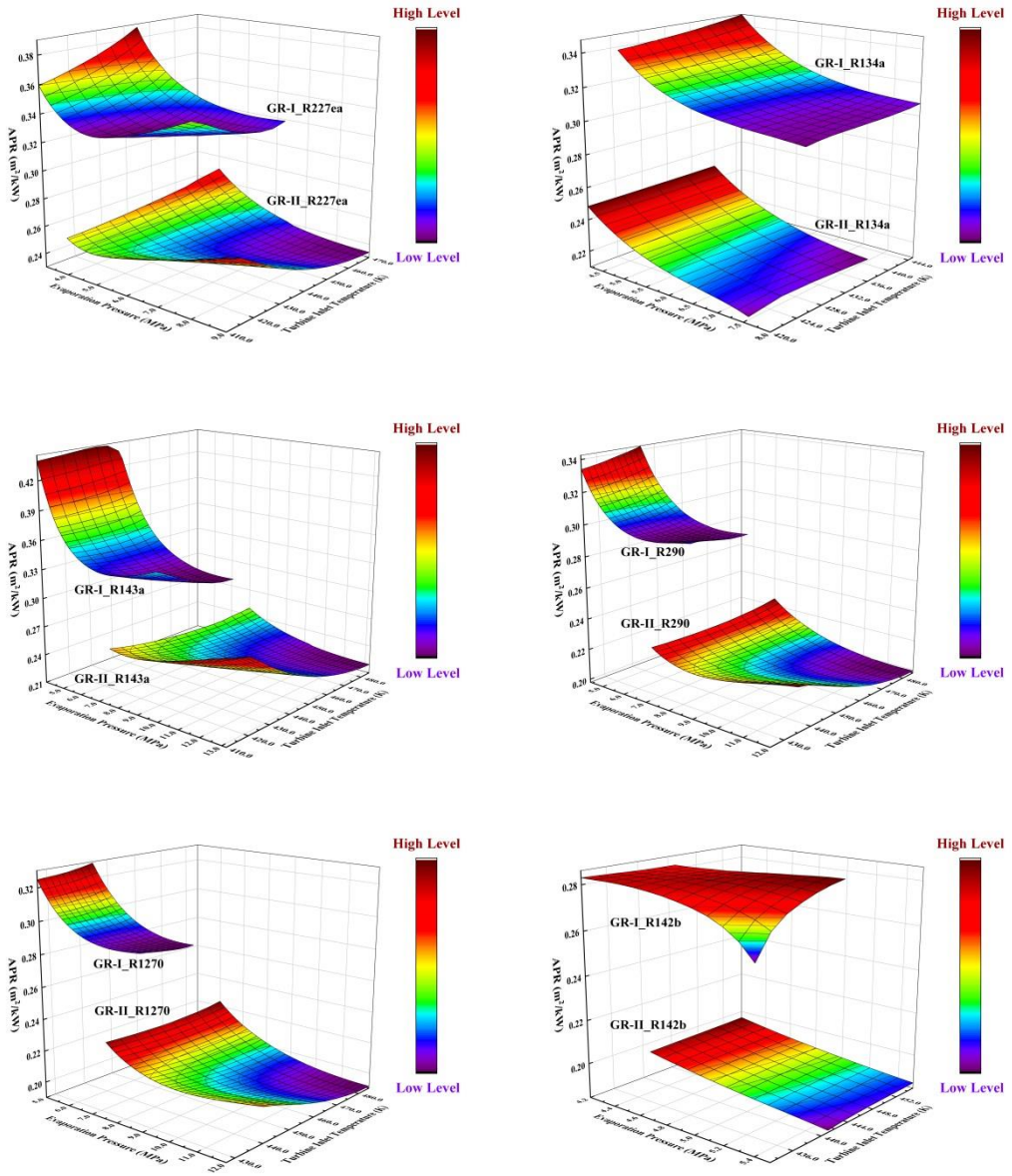

Fig. 7. Heat transfer area per net output power (APR) variation in two geothermal reservoirs

Utilizing the techno-economic evaluation model established previously, the heat transfer area per net output power (APR) and electricity production cost (EPC) are adopted for detailed illustration of the techno-economic properties of TORC system. First of all, as depicted in Figs. 7 and 8, the map alteration of two indexes for each working fluid (expect R142b) expresses consistent changing trend under the influence of evaporation pressure (P_4) and turbine inlet temperature (T_4) in the both two geothermal reservoirs. The APR and EPC values in GR-I is commonly above those of GR-II. As for GR-I and GR-II, APR ranges from 0.262-0.444(m^2/kW) and 0.185-0.290(m^2/kW). EPC ranges from 0.030-0.054($/(kW·h)) and 0.022-0.055 ($/(kW·h)), indicating that GR-II is more profitable in the techno-economic perspective. Furthermore, APR implies the compactness of heat exchangers structure which refers to the ratio of hear transfer areas of all heat exchangers to net output power. For the purpose of cutting down the overall cost of the whole system, it's better to achieve the APR as low as possible. Then, it can be seen form Fig. 7 that APR of R227ea, R143a, R290 and R1270 decreases initially before increasing in both two geothermal reservoirs when increasing P_4 under given T_4. Since the net output power (P_{net}) first increases and then decreases for the four working fluids with which trend of variation is more dramatically than the heat transfer areas change. Regarding the APR of R134a and R142b, it's decreasing yet with an increment of P_4 under given T_4. The difference of R134a and R142b from other four alternatives accounts for the downward trend of heat transfer areas varies more significantly than that of P_{net}. Moreover, the region of minimum APR for the

working fluids (expect R142b in GR-I) begins to appear when further increasing P_4 and T_4 simultaneously. Summarily, concluding from the optimal results under the operated conditions. R142b acquires the lowest APR of 0.262(m^2/kW) and 0.185(m^2/kW) in GR-I and GR-II, for 5.4MPa, 433K and 5.5MPa, 441K of the P_4 and T_4. Additionally, R227ea obtains higher APR of 0.331(m^2/kW) and 0.234(m^2/kW) respectively, for 5.8MPa, 425K and 9.0MPa, 470K.

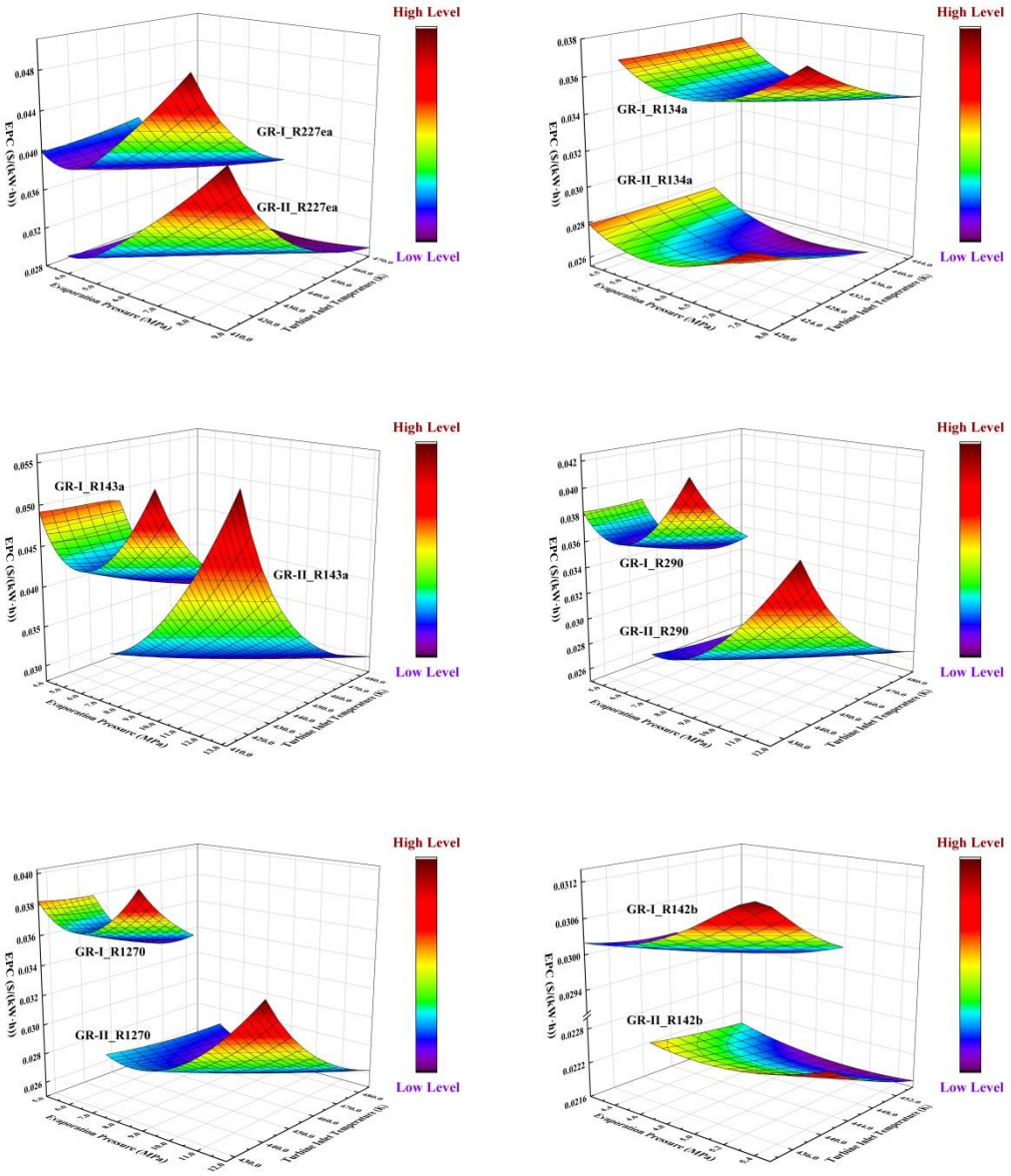

Fig. 8. Electricity production cost (EPC) variation in two geothermal reservoirs

EPC is directly proportional to the gross cost ($Cost_{2019}$) and inversely to the net output power (P_{net}) and the whole working time ($h_{working-time}$) of the TORC system. Hence, in the case of a certain $h_{working-time}$ with increasing the evaporation pressure (P_4) under given turbine inlet temperature (T_4), Fig. 8 shows that EPC exhibits a trend of decrease initially and increase afterwards for the reason that P_{net} increases first and then decreases, meanwhile, the pressure tolerance of components is required to enhance which leads to an inevitable increase in $Cost_{2019}$. Similarly, the EPC decreases firstly and then increases when increasing T_4 under lower P_4. The explanation for this variation is similar with ranging P_4 but the discrepancy exists that overall heat transfer areas keep increasing which draws an increase in $Cost_{2019}$. When considering the limits of the maximal T_4 under higher P_4, the upward tendency of EPC would not appear anymore. By comparing the optimal results between working fluids, the lowest EPC appears at R142b of 0.030($/(kW·h)) and 0.022($/(kW·h)) when the P_4 and T_4 are 4.6MPa, 445K and 5.1MPa, 455K in GR-I and GR-II. Moreover, R143a gets higher EPC of 0.040($/(kW·h)) and 0.0285($/(kW·h)) for 7.6MPa, 445K and 9.4MPa, 485K of P_4 and T_4.

3.3 Three-level fuzzy evaluation

As illustrated in maps of thermodynamic and techno-economic parameters above, the iteration outcomes can be exported by varying the tested evaporation pressure (P_4) and turbine inlet temperature (T_4) for each working fluid alternative. In the meantime, the case study regards the maximal P_{net} as objective function to obtain the optimal results for GR-I and GR-II. As listed in Tables 5 and 6, the values of the rest indexes such as η_t or APR are acknowledged under the same values of P_4 and T_4 when P_{net} gets the maximum. In this paper, the available options of scheme included R227ea (D1), R134a (D2), R143a (D3), R290 (D4), R1270 (D5) and R142b (D6). The decision criteria set is comprised of Safety Level (C1), ALT (C2), ODP (C3), GWP (C4), P_{net} (C5), η_t (C6), η_e (C7), APR (C8), SP (C9), $\mathrm{Cos}t_{2019}$ (C10), EPC (C11), DPP (C12) and SIR (C13).

Judging by the rules of criteria for higher-the-better such as C5, C6, C7 and C12 or lower-the-better involving C1, C2, C3, C4, C8, C9, C10, C11 and C13, a pair-wise comparison matrix of the P_{net} (C5) for schemes in GR-I is constructed for instance. As depicted in Table 7, it can be seen that the values on diagonal line are all 0.5 in the matrix on account of the P_{net} of each scheme is identical to itself. When it comes to comparing the P_{net} of D1 to D2, the result is 0, because of the value of P_{net} in D1 is lower than D2. Conversely, 1 is appeared when comparing D2 with D1 for the P_{net} of D2 is higher than D1. The sum of each row is got after the consistence checking between all the schemes. Arranging the sum of schemes in a descending order, those are D6, D2, D4, D5, D1 and D3. Furthermore, since the ranking is based on an interval of 0.5, D6 acquires the highest of 5.5 at the first position and the semantic score is assigned 1. D2 obtains 4.5 and scored 0.818 in the third place. The weighting is calculated by means of the semantic score for each scheme dividing the sum semantic scores for all schemes in the normalization process. Then, the weighting set for other twelve criteria are derived from the same procedures. Tables 8 and 9 list the results of weighting matrix for all schemes ($\boldsymbol{R}_i$) after normalization in GR-I and GR-II.

Table 5 Simulated optimal results of GR-I

Working Fluid	P_4 /MPa	T_4 /K	P_{net} /kW	η_t /%	η_e /%	APR(m^2/kW)	SP/m	$Cost_{2019}$ (10^5\$)	EPC(\$/(kW·h))	DPP/Year	SIR	Scheme
R227ea	6.6	445	1158.13	10.78	39.40	0.338	0.068	31.84	0.038	4.062	3.115	D1
R134a	7.6	445	1318.65	12.31	44.91	0.308	0.064	32.59	0.034	3.589	3.466	D2
R143a	9.4	445	1115.41	10.64	38.29	0.325	0.052	32.69	0.041	4.380	2.923	D3
R290	7.6	445	1265.92	11.93	43.25	0.298	0.070	32.62	0.036	3.766	3.324	D4
R1270	8.6	445	1256.59	11.90	43.00	0.291	0.064	32.58	0.036	3.794	3.303	D5
R142b	5.2	445	1513.27	14.04	51.42	0.285	0.087	32.74	0.030	3.084	3.959	D6

Table 6 Simulated optimal results of GR-II

Working Fluid	P_4 /MPa	T_4 /K	P_{net} /kW	η_t /%	η_e /%	APR(m^2/kW)	SP/m	$Cost_{2019}$ (10^5\$)	EPC(\$/(kW·h))	DPP/Year	SIR	Scheme
R227ea	8.6	470	1694.22	11.31	33.42	0.234	0.067	34.94	0.029	2.923	4.153	D1
R134a	7.4	440	1821.87	12.12	35.90	0.214	0.064	34.08	0.026	2.621	4.578	D2
R143a	13	485	1760.56	12.01	34.96	0.219	0.051	37.82	0.030	3.060	3.988	D3
R290	11.2	485	1966.04	13.28	38.92	0.199	0.068	36.98	0.026	2.637	4.554	D4
R1270	11.8	485	1981.99	13.43	39.28	0.191	0.063	37.14	0.026	2.626	4.571	D5
R142b	5.5	455	2179.54	14.43	42.89	0.187	0.087	33.98	0.022	2.146	5.494	D6

Table 7 Consistence checking, semantic score assignment and weighting calculation of net output power (P_{net}) for scheme

C5	D1	D2	D3	D4	D5	D6	Sum	Score	Weighting
D1	0.5	0	1	0	0	0	1.5	0.429	0.1133
D2	1	0.5	1	1	1	0	4.5	0.818	0.2161
D3	0	0	0.5	0	0	0	0.5	0.333	0.088
D4	1	0	1	0.5	1	0	3.5	0.667	0.1762
D5	1	0	1	0	0.5	0	2.5	0.538	0.1422
D6	1	1	1	1	1	0.5	5.5	1	0.2642

Table 8 Weighting of decision criteria for each scheme after normalization of semantic score in GR-I

	C1	C2	C3	C4	C5	C6	C7	C8	C9	C10	C11	C12	C13
D1	0.2383	0.1133	0.1806	0.1133	0.1133	0.1133	0.1133	0.088	0.1422	0.2642	0.1133	0.1133	0.1133
D2	0.2383	0.1762	0.1806	0.1762	0.2161	0.2161	0.2161	0.1422	0.2161	0.1762	0.2161	0.2161	0.2161
D3	0.1429	0.088	0.1806	0.088	0.088	0.088	0.088	0.1133	0.2642	0.1133	0.088	0.088	0.088
D4	0.1022	0.2161	0.1806	0.2161	0.1762	0.1762	0.1762	0.1762	0.1133	0.1422	0.1762	0.1762	0.1762
D5	0.1022	0.2642	0.1806	0.2642	0.1422	0.1422	0.1422	0.2161	0.1762	0.2161	0.1422	0.1422	0.1422
D6	0.1761	0.1422	0.097	0.1422	0.2642	0.2642	0.2642	0.2642	0.088	0.088	0.2642	0.2642	0.2642

Table 9 Weighting of decision criteria for each scheme after normalization of semantic score in GR-II

	C1	C2	C3	C4	C5	C6	C7	C8	C9	C10	C11	C12	C13
D1	0.2383	0.1133	0.1806	0.1133	0.088	0.088	0.088	0.088	0.1422	0.1762	0.1133	0.1133	0.1133
D2	0.2383	0.1762	0.1806	0.1762	0.1422	0.1422	0.1422	0.1422	0.1762	0.2161	0.2161	0.2161	0.2161
D3	0.1429	0.088	0.1806	0.088	0.1133	0.1133	0.1133	0.1133	0.2642	0.088	0.088	0.088	0.088
D4	0.1022	0.2161	0.1806	0.2161	0.1762	0.1762	0.1762	0.1762	0.1133	0.1422	0.1422	0.1422	0.1422
D5	0.1022	0.2642	0.1806	0.2642	0.2161	0.2161	0.2161	0.2161	0.2161	0.1133	0.1762	0.1762	0.1762
D6	0.1761	0.1422	0.097	0.1422	0.2642	0.2642	0.2642	0.2642	0.088	0.2642	0.2642	0.2642	0.2642

According to the property diversities of the thirteen decision criteria, they can be divided into three levels. The first level considers safety and environmental friendly properties which contains C1~C4. The second level concerns with thermodynamic qualities including C5~C7. As for the third level, it is made up of C8~C13 with concentrating on techno-economic characteristics. Differential from the semantic score assignment and weighting calculation of criteria in pair-wise matrix established for schemes as shown in Table 7, Table 10 summarizes the pair-wise matrix built for the three levels in GR-I and GR-II, in which the criteria are compared within the same hierarchy. E.g., ranking the relative importance among criteria in the first level, that is C3, C4, C2, and C1. Namely, when comparing C1 with C2, the result is 0 because of C1 is less significant than C2. After the consistency checking of C1~C4 in the first level and arranging the sum of each criterion in descending order, in which the ranking is identical to the importance sequence. Moreover, it is because that the ranking is based on an interval of 1.0, thus, C3 ranks first for getting 3.5 and assigned the semantic score of 1. C4 ranks second and scored 0.919 due to a sum of 2.5. For the criteria in levels two and three, the relative importance rankings are C7, C6, C5 and C11, C13, C12, C10, C8, C9 respectively. Similarly, the semantic score assignment and weighting calculation are performed the same as the first level demonstrated earlier.

Table 10 Consistence checking, semantic score assignment and weighting calculation of decision criteria for three levels

	C1	C2	C3	C4	C5	C6	C7	C8	C9	C10	C11	C12	C13	Sum	Score	Weighting
C1	0.5	0	0	0										0.5	0.739	0.2135
C2	1	0.5	0	0										1.5	0.818	0.2363
C3	1	1	0.5	1										3.5	1	0.2888
C4	1	1	0	0.5										2.5	0.905	0.2614
C5					0.5	0	0							0.5	0.818	0.3004
C6					1	0.5	0							1.5	0.905	0.3324
C7					1	1	0.5							2.5	1	0.3672
C8								0.5	1	0	0	0	0	1.5	0.667	0.141
C9								0	0.5	0	0	0	0	0.5	0.6	0.1269
C10								1	1	0.5	0	0	0	2.5	0.739	0.1563
C11								1	1	1	0.5	1	1	5.5	1	0.2114
C12								1	1	1	0	0.5	0	3.5	0.818	0.173
C13								1	1	1	0	1	0.5	4.5	0.905	0.1914

599 Referring to the last step of three-level fuzzy decision method, the final
600 evaluation results can be acquired by multiplying the weighting matrix of criteria for
601 three levels ($\boldsymbol{W}_i$) and the weighting matrix for schemes ($\boldsymbol{R}_i$). What accounts more is
602 that the first level result should be inserted as last row in $\boldsymbol{R}_i$ of the second level.
603 Furthermore, $\boldsymbol{W}_i$ for second level is multiplying 3/4 as well. And then the
604 equivalent weight needs to be assigned as 1/4 and added in the fourth position of
605 $\boldsymbol{W}_i$ in order to keep the weighting matrix dimension consistency. Repeatedly, the
606 result for the third level can be obtained by substituting 3/4 and1/4 with 6/7 and 1/7.

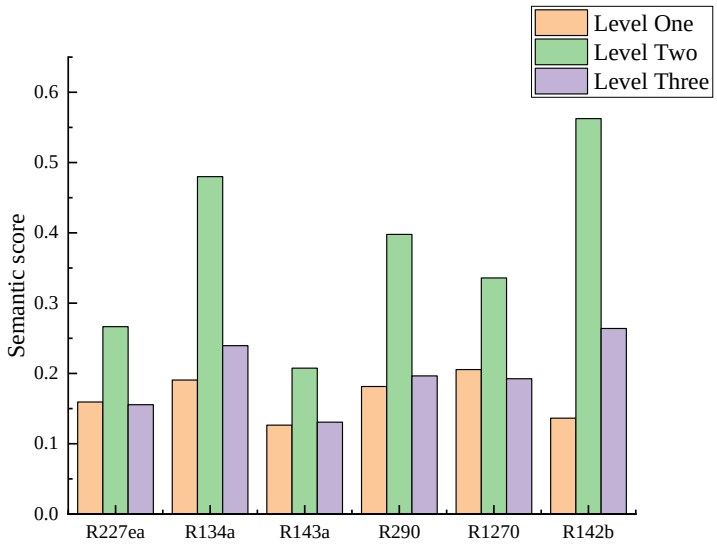

Fig. 9. Results of three-level fuzzy evaluation for GR-I

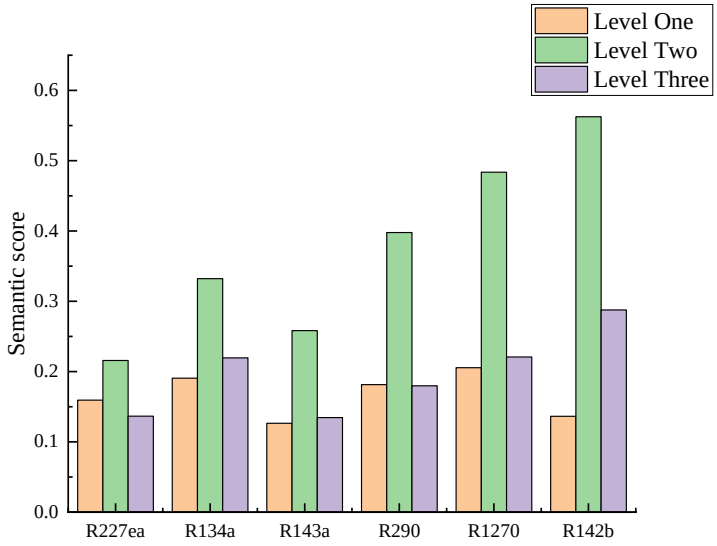

Fig. 10. Results of three-level fuzzy evaluation for GR-II

Figs. 9 and 10 exhibit the comparisons of the three-level evaluation results for GR-I and GR-II. It is concluded that the first level evaluation result are equally in the two geothermal reservoirs. R1270 possess the best reliability when only concerns about safety and environmental friendly properties. The second and third level evaluation results show that R142b is the optimal one which behaves excellent thermodynamic and techno-economic performance among selected working fluids. To the opposite, R143a is not much appropriate for the geothermal operation process according to the three-level evaluation results.

What's more, it is noteworthy that the third level evaluation result for GR-I in Fig.9 is consistent with the optimal ranking result of P_{net} in Table 5. However, comparing the result in Fig.10 and Table 6, which exerts difference between the evaluation and optimal raking order with respect to GR-II. It is implied that the impact of techno-economic indexes on the overall system performance is more apparent at high temperatures.

4 Conclusions

Based on the constructed environmental, thermodynamic and techno-economic assessment models, this paper develops a three-level fuzzy decision method for TORC system used in medium and high temperature geothermal reservoirs. The optimal results of the geothermal TORC system are obtained when P_{net} reaches the maximum. The evaluation results are gained by semantic score assignment, weighting calculation and order ranking. Both of results contribute to the following conclusions:

1. According to the first level evaluation result, the ranking of the working fluid is R1270, R134a, R290, R227ea, R142b and R143a which is identical to both GR-I and GR-II.

2. The second level takes into account the first level result and thermodynamic characteristics, ranking like R142b, R134a, R290, R1270, R227ea, R143a for GR-I and R142b, R1270, R290, R134a, R143a, R227ea for GR-II. It is concluded that R142b is both the most suitable working fluid for its maximal net output power. By contrast of the second level evaluation results for R134a in the two geothermal reservoirs, the heat source with lower temperature and pressure in GR-I is more compatible with it.

3. In terms of the third level, it takes the former two levels results and techno-economic properties into consideration. The evaluation ranking is R142b, R134a, R290, R1270, R227ea and R143a for GR-I. For GR-II ranks R142b, R1270, R134a, R290, R227ea and R143a. From the comprehensive standpoint of the three-level evaluation results, R142b is recommended as best one for the geothermal TORC systems.

The three-level fuzzy decision method developed in this work can effectively figure out the influence of a former level decision criteria on the latter one. The designers can decide on strategies and solutions according to practical requirements by adjusting weighting on indexes. It also helps the investors make whole-scale judgements in the pre-design stage of geothermal ORC system. As for the future work employed with this methodology, it can be extended to analyze the optimization process and make reliable design decisions for different ORC layout.

Acknowledgements

This research work is funded by EPSRC (EP/P028829/1) in United Kingdom.

Reference

[1] Anderson A, Rezaie B. Geothermal technology: Trends and potential role in a sustainable future. Appl Energy 2019; 248:18-34. https://doi.org/10.1016/j.apenergy.2019.04.102.

[2] Statistical review of world energy, https://www.bp.com/en/global/corporate/energy-economics/statistical-review-of-world-energy.html; 2020.

[3] Limberger J, Boxem T, Pluymaekers M et al. Geothermal energy in deep aquifers: A global assessment of the resource base for direct heat utilization. Renew Sustain Energy Rev 2018; 82:961-975. https://doi.org/10.1016/j.rser.2017.09.084.

[4] Moloney F, Almatrafi E, Goswami DY. Working fluid parametric analysis for recuperative supercritical organic Rankine cycles for medium geothermal reservoir temperatures. Renew Energy 2020; 147:2874-2881. https://doi.org/10.1016/j.renene.2018.09.003.

[5] Liang Y, Sun Z, Dong M et al. Investigation of a refrigeration system based on combined supercritical CO2 power and transcritical CO2 refrigeration cycles by waste heat recovery of engine. Int J Refrig 2020; 118:470-482. https://doi.org/10.1016/j.ijrefrig.2020.04.031.

[6] Li XY, Shu GQ, Tian H. Integrating off-design performance in designing CO2 power cycle systems for engine waste heat recovery. Energy Conver Manage 2019; 201:112146. https://doi.org/10.1016/j.enconman.2019.112146.

[7] Song J, Gu CW, Ren XD. Parametric design and off-design analysis of organic Rankine cycle (ORC) system. Energy Conver Manage 2016; 112:157-165. https://doi.org/10.1016/j.enconman.2015.12.085.

[8] Wang X, Shu GQ, Tian H et al. Effect factors of part-load performance for various Organic Rankine cycles using in engine waste heat recovery. Energy Conver Manage 2018; 174:504-515. https://doi.org/10.1016/j.enconman.2018.08.024.

[9] Madhawa Hettiarachchi HD, Golubovic M, Worek WM, Ikegami Y. Optimum design criteria for an Organic Rankine cycle using low-temperature geothermal heat sources. Energy 2007; 32:1698-1706. https://doi.org/10.1016/j.energy.2007.01.005.

[10] Astolfi M, Romano MC, Bombarda P, Macchi E. Binary ORC (organic Rankine cycles) power plants for the exploitation of medium–low temperature geothermal sources – Part A: Thermodynamic optimization. Energy 2014; 66:423-434. https://doi.org/10.1016/j.energy.2013.11.056.

[11] Astolfi M, Romano MC, Bombarda P, Macchi E. Binary ORC (Organic Rankine Cycles) power plants for the exploitation of medium–low temperature geothermal sources – Part B: Techno-economic optimization. Energy 2014; 66:435-446. https://doi.org/10.1016/j.energy.2013.11.057.

[12] Vetter C, Wiemer HJ, Kuhn D. Comparison of sub- and supercritical Organic Rankine Cycles for power generation from low-temperature/low-enthalpy geothermal wells, considering specific net power output and efficiency. Appl Therm Eng 2013; 51:871-879. https://doi.org/10.1016/j.applthermaleng.2012.10.042.

[13] Sun J, Liu Q, Duan Y. Effects of evaporator pinch point temperature difference on thermo-economic performance of geothermal organic Rankine cycle systems. Geothermics 2018; 75:249-258. https://doi.org/https://doi.org/10.1016/j.geothermics.2018.06.001.

[14] Meng D, Liu Q, Ji Z. Performance analyses of regenerative organic flash cycles for geothermal power generation. Energy Conver Manage 2020; 224:113396. https://doi.org/https://doi.org/10.1016/j.enconman.2020.113396.

[15] Cakici DM, Erdogan A, Colpan CO. Thermodynamic performance assessment of an integrated geothermal powered supercritical regenerative organic Rankine cycle and parabolic trough solar collectors. Energy 2017; 120:306-319. https://doi.org/10.1016/j.energy.2016.11.083.

[16] Wang XC, Levy EK, Pan CJ et al. Working fluid selection for organic Rankine cycle power generation using hot produced supercritical CO2 from a geothermal reservoir. Appl Therm Eng 2019; 149:1287-1304. https://doi.org/10.1016/j.applthermaleng.2018.12.112.

[17] Heberle F, Schifflechner C, Bruggemann D. Life cycle assessment of Organic Rankine Cycles for geothermal power generation considering low-GWP working fluids. Geothermics 2016; 64:392-400. https://doi.org/10.1016/j.geothermics.2016.06.010.

[18] Jankowski M, Borsukiewicz A, Wisniewski S, Hooman K. Multi-objective analysis of an influence of a geothermal water salinity on optimal operating parameters in low-temperature ORC power plant. Energy 2020; 202. https://doi.org/10.1016/j.energy.2020.117666.

[19] Mohammadzadeh Bina S, Jalilinasrabady S, Fujii H. Thermo-economic evaluation of various bottoming ORCs for geothermal power plant, determination of optimum cycle for Sabalan power plant exhaust. Geothermics 2017; 70:181-191. https://doi.org/10.1016/j.geothermics.2017.06.007.

[20] Wang JS, Diao MZ, Yue KH. Optimization on pinch point temperature difference of ORC system based on AHP-Entropy method. Energy 2017; 141:97-107. https://doi.org/10.1016/j.energy.2017.09.052.

[21] Zhou GY, Wu E, Tu ST. Optimum selection of compact heat exchangers using non-structural fuzzy decision method. Appl Energy 2014; 113:1801-1809. https://doi.org/10.1016/j.apenergy.2013.07.041.

[22] Manente G, Da Lio L, Lazzaretto A. Influence of axial turbine efficiency maps on the performance of subcritical and supercritical Organic Rankine Cycle systems. Energy 2016; 107:761-772. https://doi.org/10.1016/j.energy.2016.04.063.

[23] Martin H. A theoretical approach to predict the performance of chevron-type plate heat exchangers. Chem Eng Process 1996; 35:301-310. https://doi.org/10.1016/0255-2701(95)04129-x.

[24] Wang Z-Z, Zhao Z-N. Analysis of Performance of Steam Condensation Heat Transfer and Pressure Drop in Plate Condensers. Heat Transfer Eng 1993; 14:32-41. https://doi.org/10.1080/01457639308939809.

[25] Pioro IL, Khartabil HF, Duffey RB. Heat transfer to supercritical fluids flowing in channels—empirical correlations (survey). Nucl Eng Des 2004; 230:69-91. https://doi.org/10.1016/j.nucengdes.2003.10.010.

[26] Imran M, Usman M, Park BS, Yang Y. Comparative assessment of Organic Rankine Cycle integration for low temperature geothermal heat source applications. Energy 2016; 102:473-490. https://doi.org/10.1016/j.energy.2016.02.119.

[27] Kuo WS, Lie YM, Hsieh YY, Lin TF. Condensation heat transfer and pressure drop of refrigerant R-410A flow in a vertical plate heat exchanger. Int J Heat Mass Transf 2005; 48:5205-5220. https://doi.org/10.1016/j.ijheatmasstransfer.2005.07.023.

[28] Turton R, Shaeiwitz JA, Bhattacharyya D, Whiting WB. Analysis, synthesis, and design of chemical processes. 5th ed; 2018.

[29] Jenkins S. 2019 Chemical engineering plant cost index annual average, https://www.chemengonline.com/2019-chemical-engineering-plant-cost-index-annual-average/; 2020.

[30] Zhang C, Liu C, Wang S et al. Thermo-economic comparison of subcritical organic Rankine cycle based on different heat exchanger configurations. Energy 2017; 123:728-741. https://doi.org/10.1016/j.energy.2017.01.132.

Credit Author Statement

Na Zhang: Conceptualization, Writing, Investigation, Formal analysis

Qinggang Wang: Writing, Software, Data Curation, Formal analysis

Zhibin Yu: Funding acquisition, Validation, Review & Editing, Project administration

Guopeng Yu (corresponding author): Methodology, Investigation, Review & Editing, Supervision, Project coordination

*Declaration of Interest Statement

Declaration of interests

☒ The authors declare that they have no known competing financial interests or personal relationships that could have appeared to influence the work reported in this paper.

☐The authors declare the following financial interests/personal relationships which may be considered as potential competing interests: